DISSERTATION

THERMOPHYSICAL PROPERTY CHARACTERIZATION OF BINARY CHLORIDE SALTS FOR MOLTEN SALT REACTORS

Submitted by

Michaella S. Harris

Department of Environmental and Radiological Health Sciences

In partial fulfillment of the requirements

For the Degree of Doctor of Philosophy

Colorado State University

Fort Collins, Colorado

Fall 2024

Doctoral Committee:

Advisor: Ralf Sudowe

Alexander Brandl
Thomas Johnson
Karen Thorsett-Hill

ABSTRACT

THERMOPHYSICAL PROPERTY CHARACTERIZATION OF BINARY CHLORIDE SALTS FOR MOLTEN SALT REACTORS

Thermophysical properties are of critical importance to the successful demonstration of a molten salt reactor (MSR) as they have the most impact on the design, hydraulic function and neutronic behavior. However, there are limited data regarding complex, multicomponent salt systems and no standardized methodologies. Method development has become vital to produce reliable, experimental data to provide evidence to aid in the licensing of next generation reactor materials. Binary, non-actinide salt systems have become the primary focus as the foundation for supplying experimental data for simulations and validating new methodologies and techniques in measurements. Much research is still needed to fully understand the efficacy and viability of salt systems used for the fuel and coolant loops in the MSR. This dissertation focuses on the development of new methodologies and success and failures therewithin. In addition to providing new and adapted methods and techniques, the effects of outside influences and containments on the salt systems have been uncovered during this process.

ACKNOWLEDGMENTS

“Had to be me. Someone else might have gotten it wrong.”

- Mordin Solus, *Mass Effect 3*

The appreciation and gratitude that I have for all those that I have learned from and worked alongside throughout my educational journey is immeasurable. To think this all began with a tour of the Hanford B Reactor for extra credit in a humanities class taught by Albert Miller, who ignited the fire to study nuclear science and technology. The Chemistry Department at Central Washington University and my advisor Dr. Anthony Diaz, who helped me navigate the world of research and taught me that any data is good data because you are collecting something. I certainly would not have made it this far in my education and career without the foundation that CWU Chemistry gave me.

To my incredible committee at Colorado State University, thank you for the encouragement over my tenure at the university. My advisor, Dr. Ralf Sudowe, has been the ideal graduate mentor. Thank you for humanizing the graduate experience, allowing for growth through failures and mistakes, encouraging my partnership with the Pacific Northwest National Lab, and most importantly having an open door for all graduate students to come through and discuss anything.

Unfortunately, there are too many to name, but the incredible mentors and colleagues I have had the honor of working alongside at Pacific Northwest National Lab. Dr. Patricia Paviet whom without her support, encouragement, and guidance I would not be where I am today. My co-advisor Kyle Makovsky for treating me as an equal, letting me explore

rabbit holes in volatility studies, and for jumping in to help me through the final year of my Ph.D. The work conducted for this dissertation would not be possible without him.

I would not have survived the self-inflicted stress over the past few years without my fellow graduate students and friends at CSU. Samantha Labb, thank you for being truly authentic in everything you do in life and encouraging me to do the same. Maelle Coupannec, the work we did in the lab will never amount to the work we put into climbing rocks and exploring the Colorado wilderness. Thank you, both, for having confidence in me when I had none. To Billy and Noah, very rarely did we have serious scientific discussion and for that, I thank you.

Last but certainly not least, my incredible family who have shown unwavering support, through early mornings and cross country moves. My husband, Tyler, who decided it would be a good idea to start a relationship at the same time I started my Ph.D., thank you for seeing me through my highs and lows, being my shoulder to cry on, and in these final weeks, being an excellent father to our new daughter. My parents, in which I dedicate this work to, I will never be able to repay you for all that you have given me and ‘thank you’ will never be enough. I love you both, endlessly and all I can hope is that you can relax now that I am out of school.

DEDICATION

To my loving and enduring parents Forrest and Bridget Swinhart.

TABLE OF CONTENTS

LIST OF TABLES

LIST OF FIGURES

CHAPTER 1: PROJECT OUTLINE

1.1 Project Motivation

The aging of the United States infrastructure, the lack of accountability in global action for climate change initiatives, and the ever-growing population are all problems that could potentially be solved by the increased utilization of nuclear power. However, nuclear power does come with its own set of issues. Current US policy is a cradle to grave operation, forcing the fuel cycle to remain open, with no plans for long-term disposal or recycling of used fuel. Existing reactor technology is also becoming outdated, though a clear effort is being made to research next generation reactors for better efficiencies and higher safety regulations. At the time this dissertation was written, there are 94 licensed light water reactors (LWR) in the United States – of which 63 are pressurized water reactors (PWR) and the remaining 31 are boiling water reactors (BWR).[1] Current operating LWR's are considered generation II, generation III, or generation III+ which have enhanced safety features compared to the generation III.

The Molten Salt Reactor (MSR) Campaign hosted by the Department of Energy Office of Nuclear Energy (DOE-NE), was established to provide evidence based data to aid in the permitting and commissioning process of next generation reactors. The data cultivated from the molten salt reactor community will be added to the open-source Molten Salt Thermal Properties Database – Thermal Physical (MSTDB-TP) database.[2] To execute a safe and sustainable operation, the thermophysical properties of fuel and coolant salts need to be well understood. Though this work is conducted in collaboration with several

national labs and university partners, each project is unique in terms of methodology, material handling, salt system, and compositions being investigated.

1.2 Dissertation Goals

Standardized methods for the determination of thermophysical properties of molten salts do not yet exist, instead many of the currently applied methods vary in technique, accuracy, and parameters. For example, several methods for density measurements have been proposed, including neutron radiography, pycnometry, and the Archimedes approach. These techniques will be expanded upon in subsequent chapters. The focus of this dissertation is to establish and refine capabilities to investigate thermophysical properties of binary salt compositions and to elucidate their complex chemical behaviors. Understanding the thermophysical properties of binary salt compositions will aid in more accurate models of thermophysical and thermochemical quantities, assist in licensing of next generation reactor materials, and create a pathway to standardized methods. Sodium-potassium chloride (ClNaK) and magnesium-potassium chloride (KMgCl) are both binary systems proposed to be the foundation to more complex fuel and coolant salt compositions. By studying the binary systems and their endpoints the MSTDB-TP model parameters have been optimized for multicomponent systems. The experimental evidence provides data for better coupling in modeled simulations when other endpoint behaviors have been studied.[3, 4] In addition to the benchmark systems, increased water content will be investigated to determine the influence on thermophysical properties. Water is well known to increase the rate of corrosion in most metals used for containment, especially with increased temperatures. Water contamination could potentially result in the formation of hydrates or oxides in the salt resulting in a change of chemical

compound, having major impacts on melting temperature or other thermophysical properties. There is a change in $MgCl_2$ when contaminated with water, at higher temperatures converts to MgO, a very robust refractory material with a melting point of 2852°C.[5, 6] Trace water and other impurities could have a significant impact on the longevity of the reactor and safe operations.[7] Knowing how trace impurities impact thermophysical property measurements will provide evidence for new machine learning system for better models as mentioned previously. Thermohydraulic calculations will also be improved by this information, as well as any separations during the back end of reactor operations.[8 9]

1.3 Dissertation Overview

This work aims to provide a better understanding of the effect of water impurities on molten salts systems that could have an impact on the thermophysical properties, provide critical thermophysical property information on two binary chloride salt systems (ClNaK and KMgCl), and aid in the development of the MSTDB-TP. The hope is to provide new methodologies and improvements upon old techniques that could contribute positively to the scientific community.

Chapter two introduces the energy sector and the United States current infrastructure to highlight the importance of nuclear energy, while emphasizing the disadvantages of the current nuclear reactor fleet when compared to the next generation reactors. Chapter two aims to distinguish the relevance and significance of generation IV reactor research. Chapter three provides a detailed explanation into each thermophysical property that has been studied as a part of this work and how these properties will relate to reactor operation. Chapter four provides the relevant information in methodologies and

instrumental techniques required to complete this work.[2, 4, 10-12] Chapters two to four will offer a historical overview into molten salt reactors while describing old and new methodologies that can aid in filling in knowledge gaps in this field.

Two salt systems were the primary focus for this work, sodium-potassium chloride, and magnesium-potassium chloride. The benchmark system of sodium-potassium chloride has been well studied and multiple reports regarding physical properties on the end members, KCl and NaCl, exist.[13-15] This system was used to establish methods to determine various thermophysical properties and compared to literature values for method validation. Chapter five details all work that was conducted on the sodium-potassium chloride system. Chapter five focuses on exploratory studies and new methods developed for understanding density and vapor pressure for the ClNaK series. The optimization and refinement of high temperature drop calorimetry for the advancement of heat capacity and enthalpy measurements of ClNaK is also defined in this chapter. Chapter six details all work performed on the potassium-magnesium chloride system with an emphasis on storage and handling. KMgCl was selected for having reportedly low volatility and excellent heat transfer properties. Another focus for KMgCl studies was to prioritize the effects water content can have on the thermophysical properties. Further exploratory methods were developed for volatility and vapor pressure of KMgCl to advance understanding of chemical speciation.

Chapter seven summarizes the scientific improvements this dissertation provides, compares, and contrasts lessons learned between the sodium-potassium system and the potassium-magnesium system, and outlines a continuation to this work.

CHAPTER 2: INTRODUCTION

2.1 Infrastructure, Current Nuclear

2.1.1 Current Status of United States Energy Production and Grid Infrastructure

There has been increased interest concerning the nation's electrical grid in terms of reliable, clean energy.[16, 17] The United States has three main contributors to the power grid, fossil fuels which produce roughly 60% of electricity, nuclear at 19% and renewables at 21% (**Figure 1**).[18]

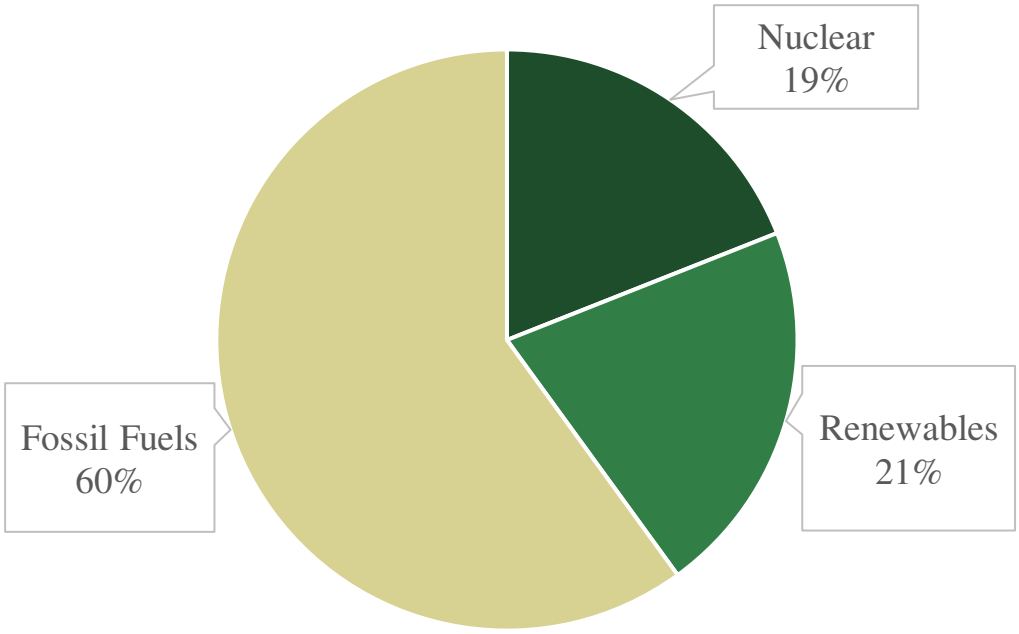

Figure 1: Pie chart reflecting 2023's energy generation by source.

Fossil fuels poses environmental concerns, with coal producing roughly 10 gigatons of CO_2 emissions in 2021, and this value is predicted to increase over time.[17]

Carbon emissions are just one factor of concern; the other is the aging transmission infrastructure that makes up the United States electric grid. The grid can be defined by

over 9200 generating units connected to 600,000 miles of transmission lines operated by an entire ecosystem of infrastructure providers. Transformers, transmission lines, and substations are outdated, susceptible to cyber-attacks, less resilient to severe weather events, and are unable to keep up with growing electrical energy demands.[19-21] Grid modernization and the Grid Resilience and Innovation Partnerships (GRIP) programs have been established to advance the resilience of the electrical grid against threats of climate change and increase the grid's reliability.[22] The new grid will need to be able to support innovative energy contributions with a heavy increase of renewables, such as wind, solar, hydroelectric, or geothermal. Renewables are defined as being a variable source of energy that has no finite source.[23] Many of these renewables have energy storage systems in place, in case of a disruption to wind or sunlight. Wind and solar do not guarantee energy production and cannot be ramped up or down as needed. For instance, - if there is no wind, turbines are unable to generate, and solar arrays produce less energy during cloudy days and none during the night. Certain renewables are able to store energy, but supplementary storage at appreciable levels is not possible from wind and solar.[24] The Great Texas Freeze caused a disruption to the grid that left people without power and water, water levels dropping in rivers are causing hydroelectric dams to drop their production rate, and new wind and hail events are damaging solar panels resulting in performance loss. All of these are examples of how extreme weather is negatively impacting energy supply to the grid.[25-28] Therefore, a clean and reliable baseline energy source, or vastly improved technology to store excess energy from renewables is still needed in the new energy grid.

In 2015, The Paris Agreement, was adopted by 196 Parties at the United Nations - recently the United States has signed to participate in the agreement. The Paris Agreement is to limit global warming by 1.5°C, with greenhouse gas emissions peaking before the year 2025, and a 43% decline in emissions by 2030.[29] The American Jobs Plan is a government initiative intended to create new jobs that includes the action items of building a renewed, modernized electric grid, as well as increasing the resiliency of the infrastructure to extreme weather.[30] Part of this plan is in conjunction with the Department of Energy to have a carbon-free power sector by 2035.

2.1.2 Nuclear Energy as the Solution

The first nuclear reactor, Chicago Pile-1, reached criticality in 1942 to aid in the Manhattan Project, and produced no electricity.[31] At the end of World War II and at the height of the cold war commercial reactors were constructed, with Shippingport going online in 1957. Since then, nuclear reactors have been supplying one fifth of America's energy.[18] Nuclear energy serves to fix many of the posed problems with climate change and increase grid resiliency. Operational Reactors have a near net zero carbon emission, a capacity factor of 92%, and use substantially less land than solar and wind farms.[32] The current nuclear fleet is not without issues. The public image of nuclear has never been favorable with weapons manufacturing, reactor accidents, and waste without a storage solution.[18] Public perception plays an important role when the construction of a new reactor is being discussed. Plans to construct new nuclear power plants are met with opposition which often delays construction or shuts down efforts to build altogether.[33, 34] These problems

need to be addressed before nuclear energy can become the main contributor to the United States power grid.

Light water reactors utilize fuel rods and boron control rods to moderate the reaction. Both BWR's and PWR's use light water as the moderator and cooling source. Water cools the reactor and is also used to generate steam to produce electricity. The difference between BWR's and PWR's is the number of cooling circuits and where the steam is generated. BWR's are based on a single loop system that boils the water, producing steam for use in the turbine and steam then condensed to repeat the process (**Figure 2**).

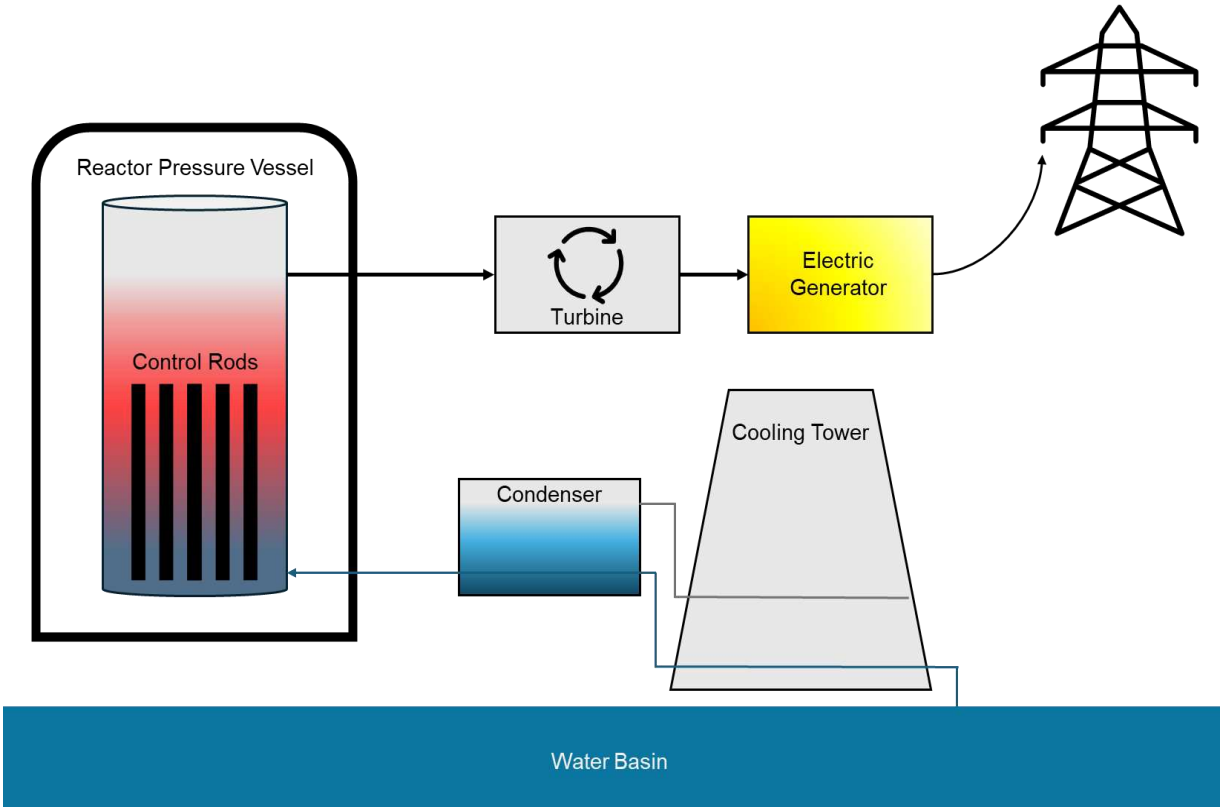

Figure 2: Adaptation of DOE diagram for boiling water reactor.

PWR's use a heat exchanger, and the steam is generated within a secondary loop, so that activated water and contaminants are contained within the primary loop. The PWR

primary loop can then be shielded to allow for better control of radioactive materials(**Figure 3**).[35, 36]

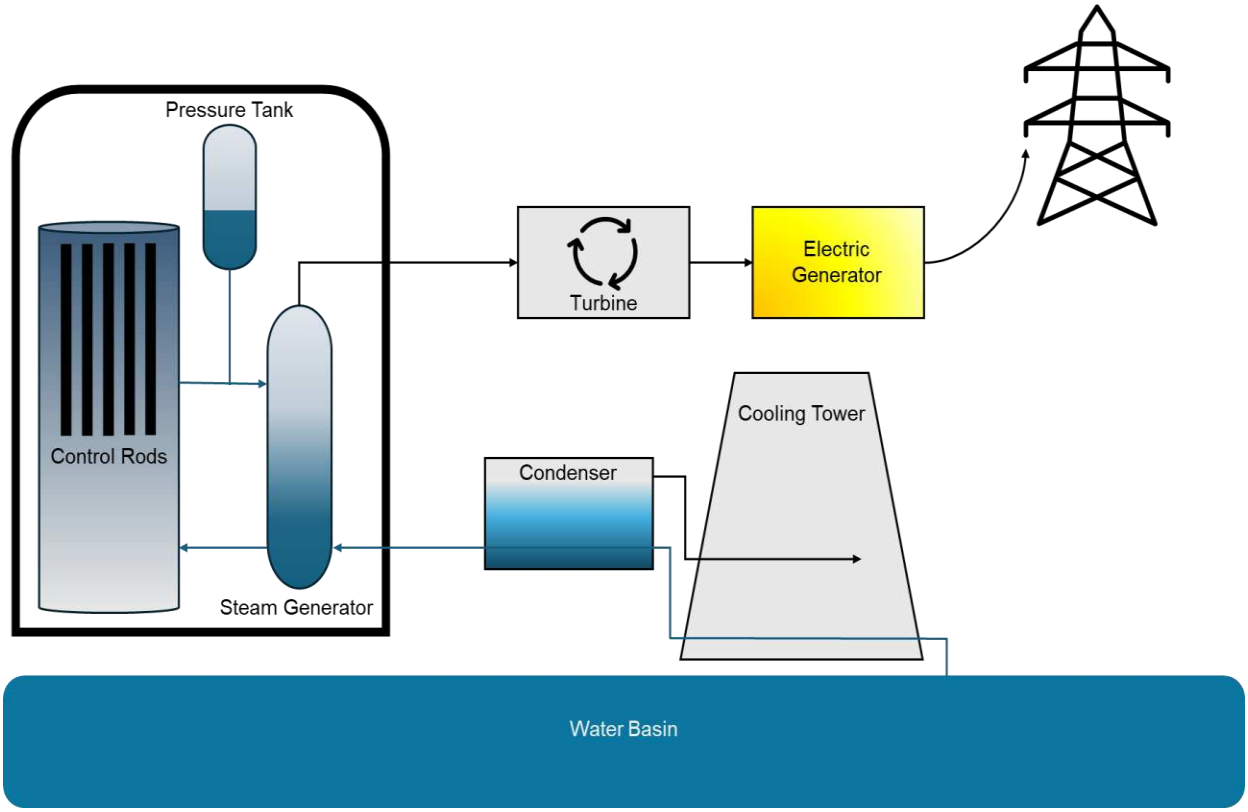

Figure 3: Adaptation of DOE diagram of pressurized water reactor.

The United States nuclear reactors currently operate with an open fuel-cycle. Natural uranium is mined, milled, converted, enriched, and fabricated into fuel pellets for light water reactors. Once the reactor is ready to be refueled every 18-24 months, the expended fuel is removed from the core and new fuel is added. The refueling outages take approximately two to three weeks to complete, and during this time the reactor is shutdown, and no electricity is produced. The old fuel is stored in cooling pools and eventually dry cask storage. Nuclear reactors in the US generate around 2000 metric tons of spent fuel per year, which is stored at various sites around the US, with no long term storage plan in place.[37] The current nuclear fleet is also aging rapidly. Vogtle units three and four, in Waynesboro, GA reached critically in 2023 and 2024, respectively and are

being advertised as “America’s first new nuclear reactors in 20 years.” Units three and four of the Vogtle plant are the first constructed and operational Generation III+ reactor in the U.S.[38, 39]

2.1.3 The Nuclear Fuel Cycle

In 2000, a committee of government representatives from nine countries initiated a discussion to begin an international collaboration to develop generation IV reactor systems. By 2016 there were 14 countries participating in the GenIV International Forum (GIF). After reviewing 100 new reactor designs, six new reactor designs and concepts were chosen by GIF to expand into the research and development stages: the Gas-cooled Fast Reactor, Lead-cooled Fast Reactor, Sodium-cooled Fast Reactor (SFR), Supercritical Water-cooled Reactor, Very High Temperature Reactor, and finally the Molten Salt Reactor (MSR). Each of these reactors have enhanced safety features and are well-suited to aid in the modernization of grid infrastructure. GIF also adopted the closed-fuel cycle model. A closed-fuel cycle adds reprocessing and recycling to the cycle instead of sending the intact used fuel to dry cask or permanent storage. Uranium can be reprocessed, or a uranium-plutonium mixture can be used as a mixed-oxide fuel (MOX), which under current regulation, is not available for use in America’s commercial reactors.[40-42]

The Plutonium Uranium Reduction eXtraction (PUREX) process is the only method that has been used by the U.S. for commercial reprocessing, and it is very efficient in separating pure uranium and plutonium product streams. Separated plutonium has the potential to be converted to weapons grade plutonium. Conversion of plutonium for use

in weapons is a major concern when addressing the suitability of the PUREX process for a future closed fuel cycle in the United States. There are four isotopes of plutonium that can be produced within a reactor, the fissile Pu-239 and Pu-241, and Pu-238 and Pu-240. The ratios in which these isotopes occur within the reactor depend on the initial fuel loading, the percentage of uranium enrichment and the irradiation time. Increased levels of $^{239, 241}$Pu makes the separated material more susceptible to proliferation, but changing the ratio to favor $^{238, 240}$Pu then makes the separated material less susceptible to proliferation.[16]

One process that has been heavily studied in the US is the UREX+ process which focuses on uranium extraction. The UREX process is almost identical to the PUREX process; however, without the portioning of plutonium. Transuranic (TRU) waste and all fission products (except technetium) are separated during the extraction process.

The Combined Extraction, COEX™, process is used in France and is a modified version of PUREX. However, because of trademark issues, information on the actual chemical process is not available. COEX™ is simplified and does not allow any pure plutonium to be extracted. The COEX™ method can be paired with other extraction methods for recycling of minor actinides.[40, 43, 44]

Both UREX+ and COEX™ are modified versions of PUREX that prevent a pure separation of plutonium. UREX+ and COEX™ are compatible with further separations to lower the amount of high level and low activity waste streams. PUREX, UREX+, and COEX™ methods are utilized in the preparation of mixed oxide fuel which can be used in LWR and in MSR's. During the separation process, in which PUREX can be adapted, pure plutonium oxide is made through aqueous polishing. Aqueous polishing starts with

weapons grade plutonium being dissolved in nitric acid and hydrofluoric acid, after which it goes through an ion exchange column to purify. Pu(IV) oxalate precipitates at 65°C after purification. The precipitate is heated in a muffle furnace to ensure the purity of the PuO_2. The PuO_2 is then mixed with depleted UO_2 to form a pellet for LWR fuel.[45] The purpose behind the proposed MOX process is to decrease the amount of desirable Pu isotopes (Pu-239, 241) in the fuel by fissioning Pu-239, 241 in a reactor. Utilizing plutonium as MOX fuel in a reactor was found to decrease Pu-239 by 40% and increase Pu-240 by 15%. MOX has the potential to decrease weapons grade plutonium stockpiles on a global scale while providing clean energy.[43] Using MOX fuel reduces the amount of waste that is currently generated and allows the spent fuel to be repurposed. Chosen for their robust design and enhanced safety features, MSR's have the ability to handle many types of fuel and can be used as burner or breeder reactors.

2.1.4 Molten Salt Reactors: Then and Now

The concept of the MSR is not new and originated in 1954 at Oak Ridge National Laboratory (ORNL) as part of the Aircraft Nuclear Propulsion Program (ANP). The proposed MSR scheme is separated into three loops: the primary fuel loop, the secondary coolant, and the steam production, power, loop. The primary loop contains the fuel salt which is actinide bearing. The secondary coolant loop, separated by the primary loop via heat exchangers, is not actinide bearing or contaminated. The power loop consists of water flow going through a heat exchange process with the coolant salt to generate steam for the turbine. MSR's have a unique failsafe in the unlikely event of an uncontrolled criticality or leak, emergency freeze tanks. Emergency freeze tanks are designed to

empty the fuel salt from the core and flash freeze the molten salt. The implementation of an onsite processing plant is a new feature to reactor designs as well. MSR's are designed to take out neutron poisons detrimental to the neutron economy and to purify the salt for continuous operations.

The fuel salts $NaF\text{-}ZrF_4\text{-}UF_4$ (FUNaZr), $^7LiF\text{-}BeF_2\text{-}ZrF_4\text{-}UF_4$ (FLiBeZr), and $^7LiF\text{-}BeF_2\text{-}UF_4$ (FLiBe) have been studied minimally in the past with conflicting reports when compared to current methods and measurements. Technology and safety regulations have changed relative to the research that was conducted during the Cold War Era. Beryllium based materials are exceptionally hazardous to human health, though still in consideration, are no longer the primary focus. Fluoride based salts are still favored for potential fuel because of the previous success, however chlorine-based salts have become of interest due to the chemical stability and the compatibility with MOX and waste type fuel components. The thermophysical properties of salt compounds are of critical importance to the design and implementation of a commercial reactor.

The next generation of nuclear power is promising in terms of climate control by having zero carbon emissions that can be supplementary to the addition of renewable energy. When renewables are unavailable due to a lack of wind, sun, or dropping water levels, nuclear power is able to produce power. MSR's are an excellent source due to the possibility of being continuously run and not having refueling outages.

CHAPTER 3: THERMOPHYSICAL PROPERTIES

3.1 Introduction

The study of thermophysical properties for molten salt reactor applications is rated as one of the top priority inputs to understand the thermodynamic and thermohydraulic calculations necessary for reactor operation.[8] The MSR design is inherently safer than LWR's as well as some gen IV reactor designs. One safety feature specific to MSR's is molten salt boiling points are much higher than for conventional nuclear fuel, significantly reducing the risk of pressure induced accidents.[46-48] The properties of the salt allow for a natural regulation of the reactor core, but without knowing the molten salt's thermophysical properties optimization of salt combinations is not possible. The importance of each property is described within this chapter to provide a clear understanding of each parameter and how it will affect the longevity of the reactor and its operation.

The most notable methodologies used to determine single properties (i.e., heat capacity, melting point, vapor pressure, density, etc.,) are described in these subchapters. Since no standardized method exists for thermophysical property measurement, a conglomeration of national laboratories and universities have formed a community to discuss progress made on the feasibility of capabilities being developed. A thermophysical roadmap has been developed by members of the scientific community and assembled by Oak Ridge National Laboratory to determine properties of critical importance and salt compositions that are understudied and for which more information

is needed.[4] Each method developed is a viable option as the community aims to create standardized methods to analyze salt systems in the future.

3.2 Roadmap

Molten salt reactors, like LWR's operate by nuclear fission chain reaction; however, due to the nature of the fuel MSR's, have an intrinsic safety quality unlike any other reactor. MSR's have a negative salt void and temperature coefficient for reactivity that allows for high power density and increased safety operations. A negative void coefficient will reduce the neutron population, and thus power, if control rods are pulled too rapidly upon start up or maintenance. The negative thermal reactivity coefficient will result in reduction in the neutron population and thus power, as temperature increases, preventing overheating. Negative void and temperature coefficients allow for minimal human intervention during reactor operation which will significantly reduce potential exposures. The thermophysical properties are of utmost importance for hydraulic calculations and also neutronic parameters.[46, 49] Behavior of any system is governed by that system's thermophysical properties, **Figure 4** illustrates the focus points for this work and the capabilites that have been deveped within, with ss, being solid solution, liq being liquidous.

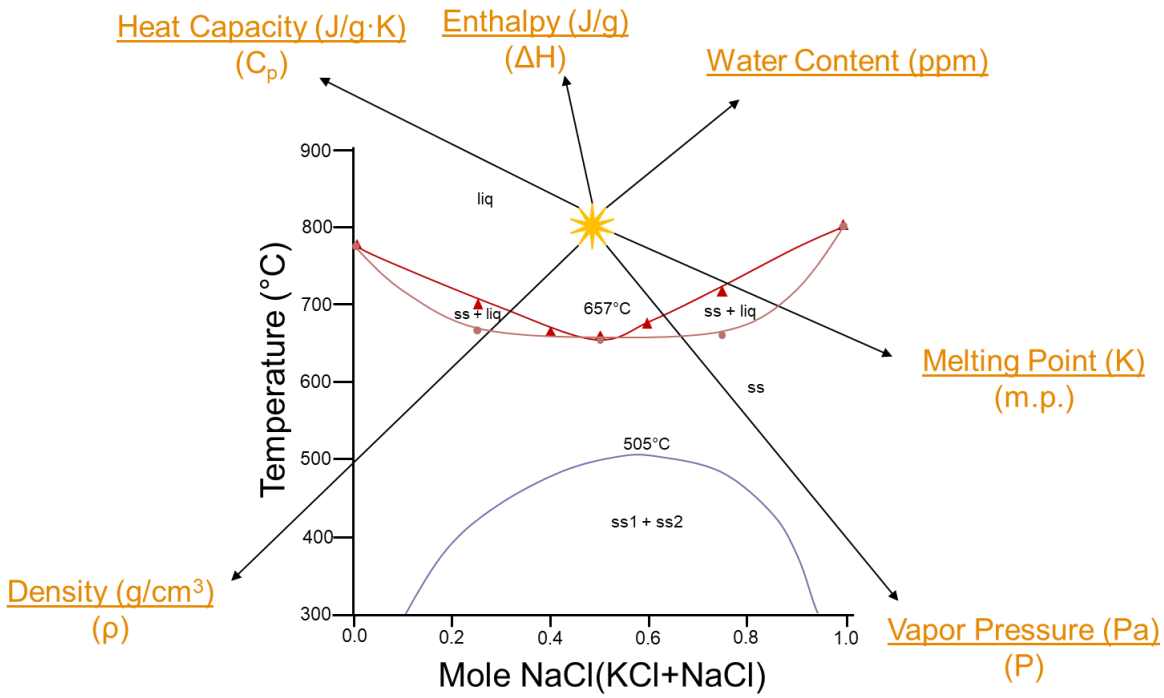

Figure 4: Roadmap illustration of the capabilities demonstrated in this dissertation, using an adaptation of a sodium-potassium chloride phase diagram.

Each property presented plays a vital role in the demonstration of a successful reactor. Testing potential salt compositions, under proposed standard operating conditions, and abnormal conditions will provide data for other methods (e.g., machine learning) to predict any event that may occur during the lifetime of the reactor.[40, 46, 50] How the molten salt behaves during operation is dependent on the thermodynamic properties of the components, many of which are covariant, but each serves an individual purpose to the importance of reactor operation. Density is crucial for the fluid dynamic behavior of the salt in the molten phase. As the density of each molten salt changes with temperature, it can circulate through the reactor creating a more tumultuous mixture. This can also cause turbulent flows within the core. With the change in density, volatility becomes an important factor.[13, 51] Previous literature and current databases show various salt systems having extremely low or negligible vapor pressures, but current research suggests the opposite

with results showing total loss of sample under high temperature.[52] Vapor pressure plays an important role when assessing critical mass for reactor operation. If salt is lost in excess headspace, actinides in the ionic form can precipitate out of the system causing adverse reactions. The thermophysical properties can also be negatively impacted by losing the non-actinide components. For example, if the binary system NaCl-KCl loses sodium chloride due to volatilization, then the starting composition of the material can change which would alter the thermohydraulic calculations required to sustain a successful operation. Finally, obtaining accurate values for the heat capacity and enthalpy for each salt chemistry is essential in understanding thermal stability. Of the properties identified above and illustrated in **Figure 4**, the most well-studied are single component salts. Systems exhibiting more complex behavior such as multi-component systems, are still lacking key thermophysical property data. Defensible values for many properties remain elusive as there is no standardized methodology, evidenced by variability and discrepancies in results between studies.[53] Furthermore, in some cases, the knowledge gaps come from antiquated datasets that often refer to unreliable measurement techniques at higher temperatures.[52] Another gap stems from the purity of the salts being used and the effects of unknown water content.

3.3 Salt Impurities

Water content, though not a thermophysical property itself, can still have a tremendous impact on the properties themselves. Investigation of water content gives insight into the proper storage and handling of various salt systems, with the purity of some being easier to maintain than others. Another aspect is how pure or dry the salts need to be to allow

for a minimally qualified operation, and what would the outcome be if degradation occurs or if water were to enter the system. Few studies have been published regarding the direct impact of trace impurities on thermophysical or thermochemical properties. One of the few studies states that oxide contamination could have impacts on the melting temperature and all other properties. This could in turn affect the longevity of the reactor, the formation of compounds, or the ability to form a unified mixture.[54, 55]

3.4 Density

Density is a vital component in determining the fluid dynamics of the molten salt system in the fuel and coolant loops.[56] Salt density decreases in a linear fashion in the molten stage with increasing temperature. This can cause a dynamic change in fluid behavior if there are hot or cold spots present within the reactor. A laminar flow is the predicted fluid dynamic of a fully operational reactor, but both turbulent and laminar flow equations rely heavily on consistent density. As more components, such as fission products, are generated during reactor operations, the density will fluctuate and an equilibrium or a steady state may be difficult to achieve.[49]

Although no standardized method to determine the density of molten salts currently exists, advancements have been made with various techniques. There are several proposed methods for determining density ranging from neutron radiography to geometric pyconometry.[14, 57] Neutron radiography begins with a collimated neutron beam that passes through several layers of various metal containments, through the sample into a scintillator; then the neutron transmission is captured with a charged-couple device camera. Using the pixel specifications from the camera, the masses of the sample

holders, and the calibrated volumes of the samples and containment, the final volume of the liquid salt at higher temperatures can be determined. Such experiments have been carried out at Los Alamos Neutron Science Center (LANSCE) at their Flight Path 5 beamline and at the CG-1D neutron beamline at their High Flux Isotope Reactor (HFIR) at ORNL. Though similar in results, both methods are conducted differently. ORNL uses quartz nuclear magnetic resonance (NMR) tubes that are vacuum sealed in an inert atmosphere to contain the samples. Samples are melted multiple times to ensure a uniform melt, and any bubbles are cleared from the liquid salt. The calculation used is derived from the Redlich-Kister (RK) Model and can only be applied to salt systems in the liquid phase. The RK model considers ideal behavior and deviation from ideal behavior for the density of the mixture. The ideal behavior can be expressed as:

$$\rho_{id} = \frac{\sum x_i MW_i}{\sum \frac{x_i MW_i}{\rho_i}} \quad \text{(Eq. 1)}$$

Where ρ_{id} is the density with ideal behavior, MW_i is the molecular weight of the compound i, and x is the mole fraction of the compound i. The expression for deviation from ideal behavior is defined as:

$$\rho_{ex} = x_A x_B \sum_{j-1}^{n} L_j (x_A - x_B)^{j-1} \quad \text{(Eq. 2)}$$

Where j is the order of expression, and L is the linear temperature expression between the binary interaction of A and B.[14, 58]

LANL uses custom stainless-steel tubes with a welded endcap and plug to seal the sample. The samples are prepared in an argon atmosphere glovebox. The furnace and imaging setup is also customized for the beam to have an unobstructed shot through the setup. The entire system is designed to have complete containment to work with plutonium samples and to operate with as little human intervention as possible. The

density is calculated using the expansion coefficients from the stainless-steel crucible and based on the initial dimensions measured. This study accounts for the meniscus height visualized in the images. The final calculation used to determine the density from the neutron images in relation to temperature is:

$$\rho(T) = M \cdot (\pi[r_0(1 + a_{ss}(T) \cdot \Delta T)]^2 \cdot [l(1 + a_{ref}(T) \cdot \Delta T)]^{-1} \quad \text{(Eq. 3)}$$

where M is the mass of the liquid, r_0 is the inner radius of the sample holder, a_{ss} is the thermal expansion coefficient of the stainless steel, T is the temperature in Kelvin and, l is the height of the meniscus.[59]

Many laboratories use a customized setup based on the Archimedes principle. Typical systems use large volumes of a reference liquid or the salt sample with a bobber attached to a balance. Numerous corrections are applied to measure the displacement of the liquid based on the mass of the bobber in the molten salt to determine the density. Archimedes methods require large amounts of salt samples and are destructive to the salt, making these measurements harder to adapt to radiological containment requirements. Similar to the Archimedes method, a geometric pycnometry method was used for this work. The benchtop version utilizes a muffle furnace in which crucibles with a calibrated inner volume filled with sample are brought to the target temperature and allowed to overflow. Another version of gravimetric pycnometry uses a thermomechanical analyzer (TMA) and a custom fabricated nickel crucible with a calibrated inner volume. In both versions of the method the displacement of salt was measured to determine the volume, and the final mass was divided by the volume to achieve the density. Many of these methods and older published data are however results of non-calibrated measurements or rough estimations of mass or displacement.

3.5 Vapor Pressure and Volatility

The National Institute of Standards and Technology (NIST) and the Joint Army-Navy-Air Force (JANAF) working group compiled databases for thermochemical and thermophysical properties of varying materials and compounds. The JANAF tables for vapor pressure and volatility of single component salts were last updated in 1974 with the methodologies from studies by Rodebush and Dixon (1925) and Fiock and Rodebush (1926). One can acknowledge that, at the time in which these studies were conducted, the techniques used were considered state-of-the-art; however, it is likely modern methods are more robust and thus may provide more accurate data on the vapor pressure of the materials of interest. The following examples highlight some of the potential problems in utilizing the methods therein, revealing limitations from these techniques spanning hundreds of degrees below and above a proposed salts melting point.

The Rodebush and Dixon method describes a supply of nitrogen to a system at a higher vapor pressure than the material being measured is predicted to have. The authors expressed concerns with the validity of this experiment at higher temperatures, stating the glassware would become dark and cloudy, making the apparatus difficult to read (**Figure 5**).

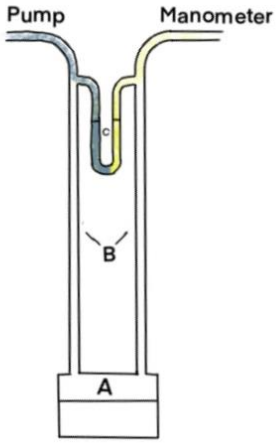

Figure 5: Drawing adapted from Rodebush-Dixon[52] apparatus. A) Thermocouple/heating block. B) Quartz tubing with enough length to stay cool when placed in the furnace. C) Differential manometer containing paraffin oil.

The NIST database also uses a method that was developed by Barton and Bloom (1956), using a bubbler. An insulator was placed within the tube containing the sample at an approximated depth and inserted into the furnace. Nitrogen then flowed into the insulator at a rate of two bubbles per second to prevent superheating, which was previously a problem in the boiling point method. Their method attempted to control temperature variance with various glass wools and insulators, the solidification of the molten salt, and to stabilize the pressure in the system [51]. The vapor pressure was measured when the thermocouple reached the boiling point temperature; however, they stated the temperature would continue to rise, indicating that the temperature reading could be incorrect for the corresponding vapor pressure.

The NIST database also uses a compilation of data that was assimilated by Stull (1947) who collected data from private sources and literature values that were available in the late 1940s. The various methods are not described in the paper and Stull (1947) states: “The personal error is also an unknown factor,” (Stull, 1947).

Miller and Kursch (1955) appear to be the first to attempt a new method that challenged the Rodebush and Dixon (1925) method. Their method used a magnetic resonance beam to detect vapor pressure. The beam measured the vapor escaping through a small slit in the source. A velocity spectrum was produced and analyzed to determine the vapor pressure. Their method was also able to detect dimers and trimers of elements, and their dissociation energy. [60]

Ewing et al. (1974) first tested NaCl using a Knudsen cell at temperatures below the melting point and states the acceptance of the JANAF tables. The Knudsen cell method is primarily used to measure vapor pressures of solids with assumed low vapor pressures. Vapor effuses through a hole and the loss of mass is proportional to the vapor pressure [61, 62]. During the isothermal process of the experiment, excess vapor is evacuated into a chamber and the mass change recorded. By measuring the rate of vaporization, the vapor pressure of the salt could be resolved.

Modern methods, such as thermogravimetric analysis (TGA), are similar to the Knudsen Cell method which measures mass loss with temperature variance but allows a much more sensitive technique that can detect micro changes. An evolved gas analyzer (EGA) offers the ability to determine rate of vaporization and can detect the gas species being released from the system itself. The EGA and TGA methodologies allow for further understanding of the ionic behavior of different salt systems, that, when applied to molten salt reactors offers an accurate change in composition that can become crucial when determining critical masses for the reactor core.

3.6 Enthalpy and Heat Capacity

Specific heat capacity, as with all other thermophysical properties, is important to the thermal hydraulics of fuel systems. A high heat capacity allows the reactor regulate neutron population in relation to the negative thermal coefficient of reactivity. The high heat capacity will moderate the neutron population changes as the temperature upon startup will be slow to increase, therefore providing a smoother transition with heat generation.[49]

Calorimetry is the most accepted method to determine specific heat capacity and molar enthalpy. Differential scanning calorimetry (DSC) and the lesser used drop calorimetry are the most common techniques used to measure enthalpy. Samples are either hermetically sealed or laser welded into metal crucibles made from, but not limited to, molybdenum, stainless-steel, or Hastelloy's. Calorimetry methods have proven to be very accurate compared to previous literature values; however, uncertainty propagation is rarely discussed in detail. Calorimetry methods are also not standardized and can vary by instrument used, sample containment, and sample preparation.

CHAPTER 4: INSTRUMENT THEORY

4.1 Thermogravimetric Analyzer

4.1.1 Theory

Thermogravimetry measures the mass change of a material as a function of temperature. The instrument depicted in **Figure 6** shows the components in a TA Instruments SDT Q600 (Waters Corp, New Castle, DE).

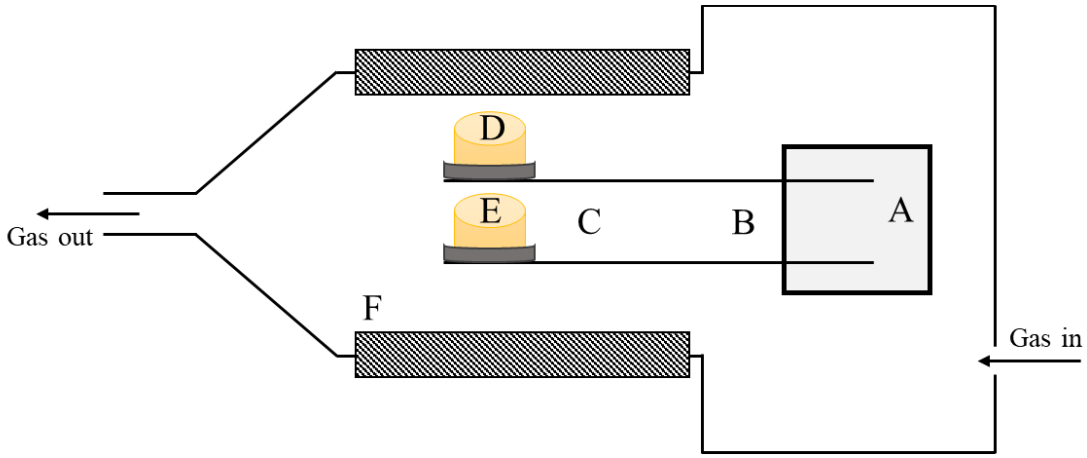

Figure 6: Thermogravimetric Analyzer Schematics. A) the controller B) Balances C) Thermocouple Rods D) Reference Pan E) Sample Pan F) Heater

The system is attached to a purge gas of breathing air, nitrogen, or argon, the flow of which can be adjusted in mL/min increments. The detectors connected to the beams act as balances to determine the mass change relative to the reference pan. The changes in mass recorded by TGA analysis can be used to interpret changes in physical characteristics of the sample, e.g., oxidation and volatilization. A method from a previous study was modified to accommodate the volatile nature of the molten salts.[63] In preliminary experiments the salt exhibited corrosion on the crucible and instrument along with total sample loss prior to the isothermal hold at higher temperatures. Samples were

analyzed at 750-900°C in a condensed breathing air atmosphere. To reduce corrosion and total sample loss the sample was placed in the TGA at room temperature and set to equilibrate at 30°C. From there, the sample was rapidly brought to the desired temperature, referred to as a jump (typically 10°C/s), and held for one hour. Pure sodium chloride and potassium chloride were used as the benchmark for this methodology, NIST Antoine values were used for A, B, and C values in Equation 4.

$$\ln p = A - \frac{B}{C+T} \quad \text{(Eq. 4)}$$

Where p is pressure (Pa), A, B, and C, are NIST Antoine constants for a specified temperature range, and T is the absolute temperature of the sample (K).

Thermogravimetric analysis is based on the Langmuir adsorption model which applies to evaporation of a material under a constant vacuum (Eq 5-8).

$$\left(\frac{1}{a}\right)\frac{dm}{dt} = p\alpha\sqrt{\frac{M}{2\pi RT}} \quad \text{(Eq. 5)}$$

Where dm/dt(a) is the rate of mass loss per unit area (kg/s·m^2), p is vapor pressure, α is the vaporization coefficient, M is the molecular weight of the vapor of the evaporating compound (kg/mol), R is the ideal gas constant (J/K·mol), and T is the absolute temperature (K). Under vacuum α is assumed to be 1 and is constant for any material being measured. Equation 5 can then be rearranged to Eq 6-8.

$$p = kv \quad \text{(Eq. 6)}$$

p is pressure, k represents the gas vapor relative to the vaporization coefficient, and v is the mass loss in terms of the surface area of the sample relative to the vaporization coefficient. The gas vapor, k, is used as a calibration constant that can be determined using the TGA to calculate a known vapor pressure. Using the experimentally determined k value, the vapor pressure of other unknown materials can be determined.

$$k = \frac{\sqrt{2\pi R}}{\alpha} \quad \text{(Eq. 7)}$$

$$v = \left(\frac{1}{\alpha}\right)\left(\frac{dm}{dt}\right)\sqrt{\frac{T}{M}} \quad \text{(Eq. 8)}$$

A graph can then be used with ln(p) from Eq. 4 against Eq. 8 to create a Clausius-Clapeyron plot with Eq. 9.

$$\ln p = A - \frac{\Delta H}{RT} \quad \text{(Eq. 9)}$$

where A is the surface area, ΔH is the change in enthalpy, R is the ideal gas constant, and T is the absolute temperature. When plotted and calculated correctly, the slope of ΔH/R will be a straight line.

4.2 Evolved Gas Analyzer Mass Spectrometry

4.2.1 Theory

Evolved gas analysis mass spectrometry (EGA-MS) was also used to determine volatilization of the salts. EGA-MS is sometimes referred to as residual gas analysis (RGA). Mass spectrometry is used to measure the masses of atoms and/or molecules being released from the sample; these masses are then used to interpret the species present. Species analysis is done by utilizing mass-to-charge ratios (m/Z). For example, an atom with a mass of 10 amu will be measured at mass 10 in the mass spectrum if the ionized atom has a charge of +1. Conversely, it would be measured at mass 5 in the spectrum if the ionized atom has a charge of +2. Ideally, ionization in the mass spectrometer design creates ions of charge +1 so that the m/Z ratio measured in the spectrum is equivalent to that of the mass of the atom or molecule.

Mass spectrometry instruments can be used to analyze solid, liquid, or gaseous samples. EGA is used to determine the components within a gas or off-gases of a system. The evolved gases are delivered to the ion source with an overflow gas, typically argon or nitrogen. The EGA uses electron impact as the ionization source, which is one of the oldest methods of ionization. Electron ionization can be described as a beam of electrons, formed by a heating a filament (-70 V), and targeting the vaporized molecules while being under a vacuum of 10^{-7} torr.[64] The kinetic energy of the electron beam (70 eV) must exceed the ionization energy of the sample molecules for ionization to occur with this method. Electron ionization will cause the ions to fragment and is primarily used for gas related mass spectrometry. After electron ionization, the fragmented gas ions are focused by a series of metallic plates, whereby collimation is achieved by applying an electrical potential across the plates. The collimated ion beam is then accelerated through the mass filter, in this case a quadrupole design. The rods contained within a quadrupole mass filter act as electrodes. Two rods are connected to the positive side and the other pair is connected to the negative terminal which accelerates the ions. The quadrupole filter used here is calibrated to allow the passage of ions with masses between 0-200 amu. The filter is adjustable based on the high-pass and low-pass filters to sort through the ions of interest. There are two types of detectors used, a sensitive electron multiplier detector and a much less sensitive Faraday Cup. For the Faraday cup, an ion beam strikes a collector electrode surrounded by a Faraday cage that prevents the escape of reflected and ejected electrons, respectively. Both the electrode and the cage are connected to a resistor that allows for a voltage drop across a resistor that minimally amplifies the signal.

The Faraday cup is typically used for a higher flow of gas, such as an overflow gas, as it will oversaturate the electron multiplier.[65]

An electron multiplier consists of a resistive conductive surface that the electrons strike causing a cascading effect to amplify the electron signal. The electrons that strike near the entrance eject secondary electrons that are attracted to the higher voltage farther within the tube. The amplified signal and cascade of electrons are able to provide quicker response times and a highly sensitive measurement.[65]

4.2.2 Operation

The Hiden Analytical HPR-20 R&D EGA (Hiden Analytical Ltd., Warrington, U.K.) is connected to a furnace using their heated Quartz Inert Capillary (QIC).[66] The system is purged and supplied continuously with argon or nitrogen depending on the mass numbers of interest. The salt samples were ramped at a rate of 10ºC/min to the desired temperature and held for analysis until the sample was in liquid form. A continuous mass scan of predicted elements was programmed alongside a camera to have pictures taken every minute to capture the salt transformation across the liquidus. Once in the liquid state, a mass scan from 0 to 150 amu was taken to determine all components potentially being released by the salt. A Faraday scan was used for all components present in high concentrations and a secondary electron detector was used for a more sensitive scan. Argon gas with a flow rate of 50 mL/min was used throughout the experiment to protect the sample from interacting with the atmosphere. The measured intensity of the Ar-40 peak was used to normalize all measured peaks. A capillary line attached to the furnace

and the EGA was held at 200°C to reduce the risk of plating the material within the line (**Figure 8**).

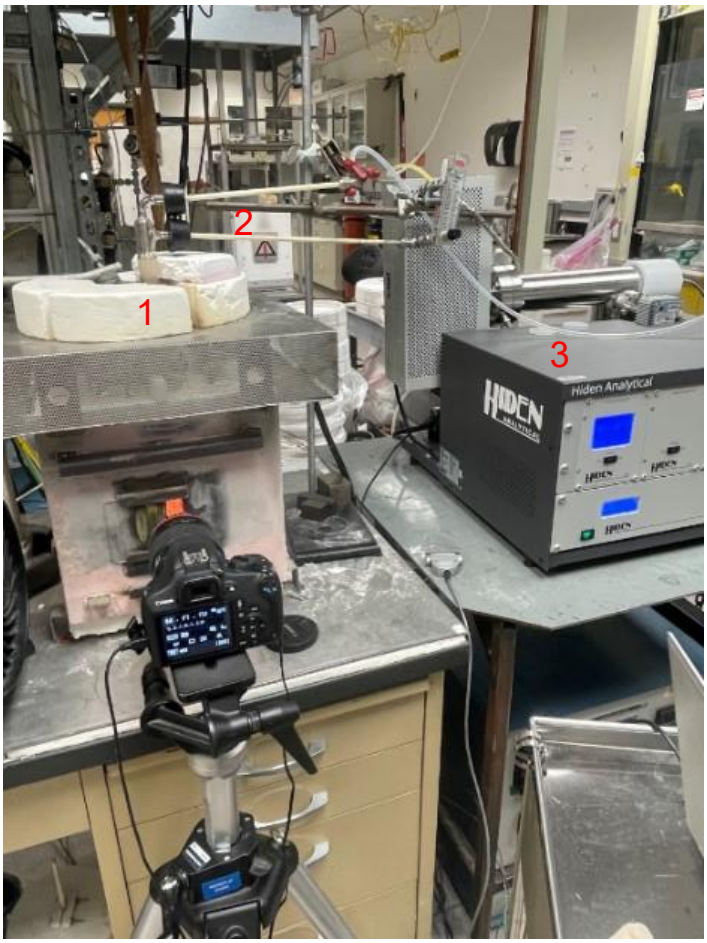

Figure 8: EGA setup 1) Furnace, 2) non-heated transfer line, 3) EGA instrument

4.3 High-Temperature Drop Calorimetry

4.3.1 Theory

High temperature drop calorimetry (HTDC) is a technique that can measure heat capacity [C_p, J/(mol·K)] and standard enthalpy ($H°$). The HTDC system used here was a Calvet DC Alexsys (Setaram, KEP Technologies, France) (**Figure 9**).

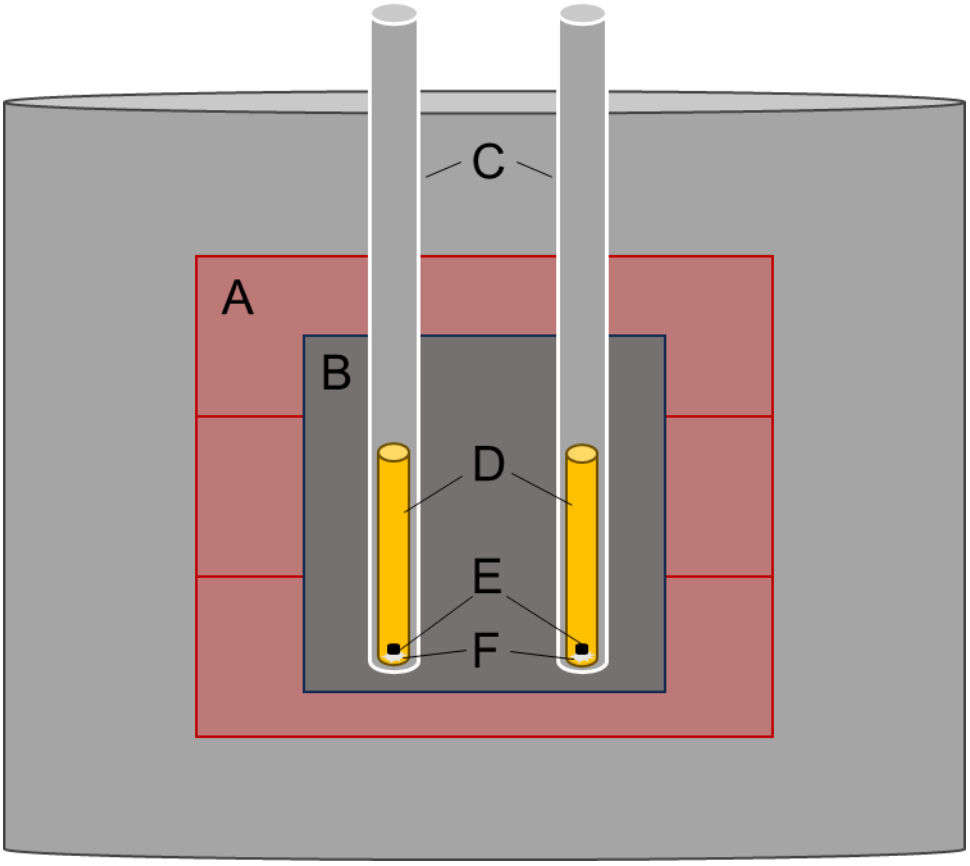

Figure 9: Drop calorimeter schematic A) temperature control zones, B) thermopiles and thermocouples, C) quartz cells containing thin drop tube, D) additional quartz tube, E) sample, F) alumina powder.

The drop calorimeter can indirectly measure standard enthalpy by using a correction factor derived from Shomate's equation for enthalpy (Eq. 10).

$$H^\circ - H^\circ_{298.15} = A*t + B*t^2/2 + C*t^3/3\ D*t^4/4 - E/t + F - H \qquad \text{(Eq. 10)}$$

where H° is the standard enthalpy of the solid or liquid state depending on the temperature profile (kJ/mol), $H^\circ_{298.15}$ is the enthalpy under standard state conditions (kJ/mol), A-H are standard values listed for the specific compound from NIST given a range of temperatures (K), and t is the temperature of the sample divided by 1000 (K). The alphabetical numbers are standardized and can be found in the NIST Chemistry WebBook (**Table 1, 2**).[67-70]

Table 1: NIST Shomate Equation constant values prior to melting temperature.

	NIST Values KCl	NIST Values KCl	NIST Values $MgCl_2$	NIST Values NaCl
A	35.41597	-717.3845	78.30733	50.72389
B	70.03472	1247.861	2.435888	6.672267
C	-91.38233	-708.5144	6.858873	-2.517167
D	52.52426	141.4435	-1.728967	10.15934
E	0.15346	103.6712	-0.729911	-0.200675
F	-449.1357	1.760084	-667.5823	-427.2115
H	-436.6841	-436.6841	-641.6164	-411.1203

Table 2: NIST Shomate Equation constant values for melting point and higher

	NIST Values KCl	NIST Values $MgCl_2$	NIST Values NaCl
A	73.59698	92.048	-42.44780
B	0	-0.000005	113.52600
C	0	4.768900×10-7	-43.64660
D	0	1.135690×10-7	5.89663
E	0	-0.000005	39.13860
F	-443.7341	-634.343	-305.56100
H	-421.7932	-601.577	-385.92300

4.3.2 Operation

Custom designed and fabricated nickel crucibles (Pacific Northwest National Laboratory, Richland, WA) were used to withstand the corrosive nature of the salts. Using an iWeld laser welder (LaserStar Technologies, Orlando, FL) crucible lids were welded to seal the salt contents and prevent leaching or volatilization of the salt during the experiment (**Table 3**).

Table 3: Operational settings for laser welding nickel crucibles.

Operational Parameters	**Setting**
Volts	230 V
Pulse Length	2.0 mS
Pulse Rate	2.0 Hz
Beam Diameter	0.20 mm

The following protocols were used for analysis via HTDC. The three temperature control zones are set to hold at a target temperature and left to reach equilibrium at the target temperature for 24-48 hours. When equilibrium has been achieved between the temperature control zones, a background measurement is performed to establish instrumental noise. The background measurement is collected for a typical length of an experimental run, twelve hours for lower temperature ranges (300-600ºC) and eight hours for higher temperature ranges (700-1000ºC). This background measurement determines roughly when the sample should be dropped during the experiment. For example, if the empty background taken at 400ºC reads 9 μV·s, then subsequent samples after the first one should be dropped when the signal returns to 9 μV·s. After the background was established a baseline run took place with three welded empty nickel crucibles. The baseline refers to the empty crucible signal that will later be subtracted from the total sample signal to determine the isolated salt signal only. Each crucible was dropped in intervals after reaching the original background measurement. The instrument was set to take a background measurement for 30-45 minutes to achieve a constant baseline that needs to be reached after a drop and before dropping the subsequent sample. This baseline measurement provides a correction for the nickel sample holder to be subtracted from the sample signal. Sample drops were performed in the same manner as baseline drops. A background measurement was achieved before and after dropping the samples, as displayed in **Figure 10**.

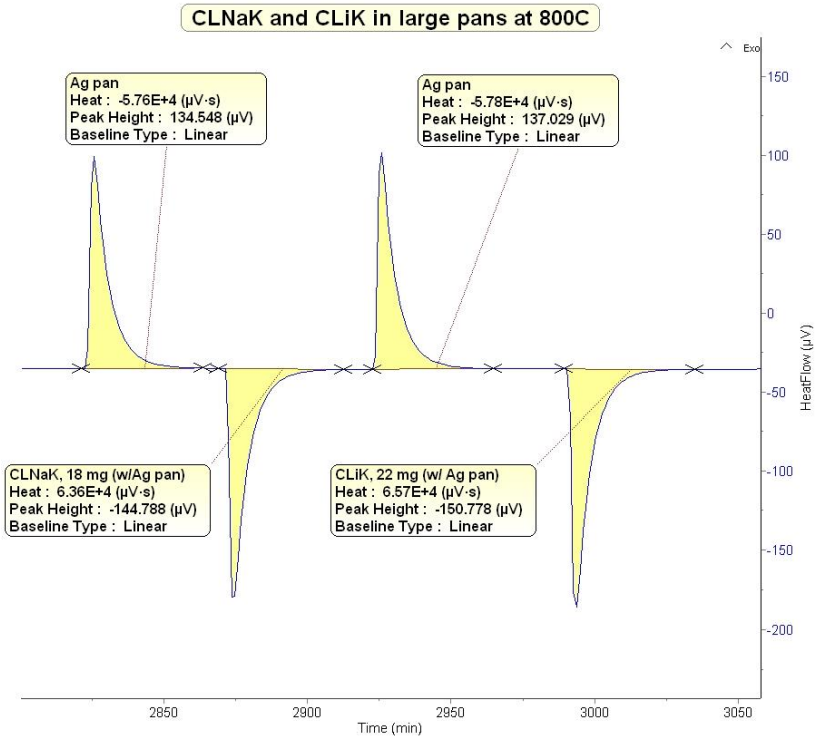

Figure 10: Example of drop calorimeter experimental output during an experiment.

The software, Callisto Processing (Setaram, KEP Technologies, France), has a peak integration function which is used to determine the total signal from the crucible. Though the calculation is programmed, determining the start and end point of the peak is done manually with much variation between users and samples. Once the peak integration is done, a series of calculations are performed to determine specific enthalpy, ΔH (Eq. 12-16).

$$B_t / B_p = B_s \qquad \text{(Eq. 12)}$$

where B_t is the baselines total integrated signal (µV·s), B_p is the baseline pan mass (mg) and B_s is the baseline signal (µV·s/mg). All baseline signals are then averaged together, $\overline{B_s}$.

$$\overline{B_s} \cdot M_p = S_p \qquad \text{(Eq. 13)}$$

where M_p is the mass of the empty sample pan (mg) and S_p is the signal from the sample pan (μV·s). The signal from the sample pan is then subtracted from the total signal S_t (μV·s), to give the sample signal S_s (μV·s).

The formula weight, F (g/mol) is the total mass of the compound that has been corrected using the molar ratio of the salt: (74.55 g/mol · 0.43) + (95.21 g/mol · 0.57) = 86.33 g/mol KMgCl4357. The moles of KMgCl compound are calculated by using the sample mass, M_s (g). Equation 10 was used to calculate the enthalpy for each endmember at the recorded room temperature and recorded drop calorimeter temperature. The enthalpy corresponding with the molar ratio of the composition for the recorded room temperature and recorded drop calorimeter temperature was then calculated.

$$(H_{room} \cdot \text{mol\% KCl}) + (H_{room} \cdot \text{mol\% } MgCl_2) = H_{room}\ KMgCl \quad \text{(Eq. 14)}$$

$$(H_{drop} \cdot \text{mol\% KCl}) + (H_{drop} \cdot \text{mol\% } MgCl_2) = H_{drop}\ KMgCl \quad \text{(Eq. 15)}$$

The total enthalpy for the sample is then calculated:

$$(H_{drop} - H_{room}) \cdot \text{moles of KMgCl} \cdot 1000 = H_{total} \quad \text{(Eq. 16)}$$

A conversion factor, CF, is made specific to the salt composition H_{total} / S_s = kJ/μV·s and used to determine the specific enthalpy, $(S_s \cdot CF) / (M_s / 1000) = \Delta H$ (kJ/mol).

4.4 X-ray Diffractometer

4.4.1 Theory

A Bruker D8 X-ray Diffractometer (XRD) (Bruker, Billerica, MA) was used for data acquisition. The instrument is equipped with a high efficiency turbo x-ray source (TXS-HE) (Bruker, Billerica, MA),and a copper K-α_1 anode that has an x-ray wavelength of 1.541 Å (0.1541 nm). A tungsten filament generates an electron beam that hits the copper

anode, generating x-rays. The resulting x-ray beam passes through a beryllium window at incident angle θ to the sample. The diffracted x-ray beam from the sample travels through a series of slits and monochromators at the reflected angle θ to the detector, for a total angle of 2-theta (**Figure 11**).

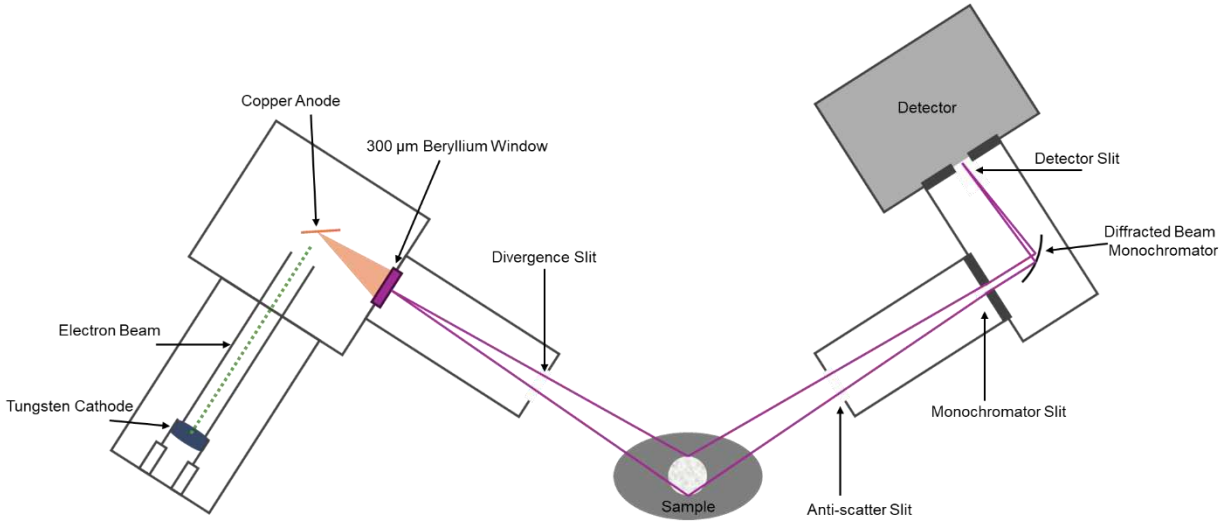

Figure 11: Adaptation of the Bruker ATLAS™ goniometer and high efficiency turbo x-ray source schematics.[71]

The x-rays are generated from the deexcitation of electrons transitioning to a lower energy orbital. The copper anode produces characteristic K-α_1 and K-α_2 x-rays at 1.541 Å. Specific to copper, the electrons release energy after being exited and relax into the K shell, the closest shell to the nucleus, α corresponds with the electrons coming from the L shell the second closest shell to the nucleus, and the one and two indicate different subshells.[72] The characteristic x-rays of copper can then be used as the wavelength in Bragg's Law (Eq. 17)

$$n\lambda = 2d\sin(\theta) \qquad \text{Eq. 17}$$

where n is the diffraction order, λ is the wavelength of the x-ray, d is the lattice distance, and θ is the angle of diffraction. The use of XRD is well established for the

characterization of crystalline solids for both phase analysis and structure determination. The diffracted x-rays that are detected produce characteristic peaks for crystalline materials with varying peak intensities if the material contains multiple compounds. Additionally, the structure, or unit cell and bond lengths can be determined by the angles of diffraction from the material.[73, 74]

The same instrument theory can be applied for the MTC-HIGHTEMP non-ambient stage (**Figure 12**).

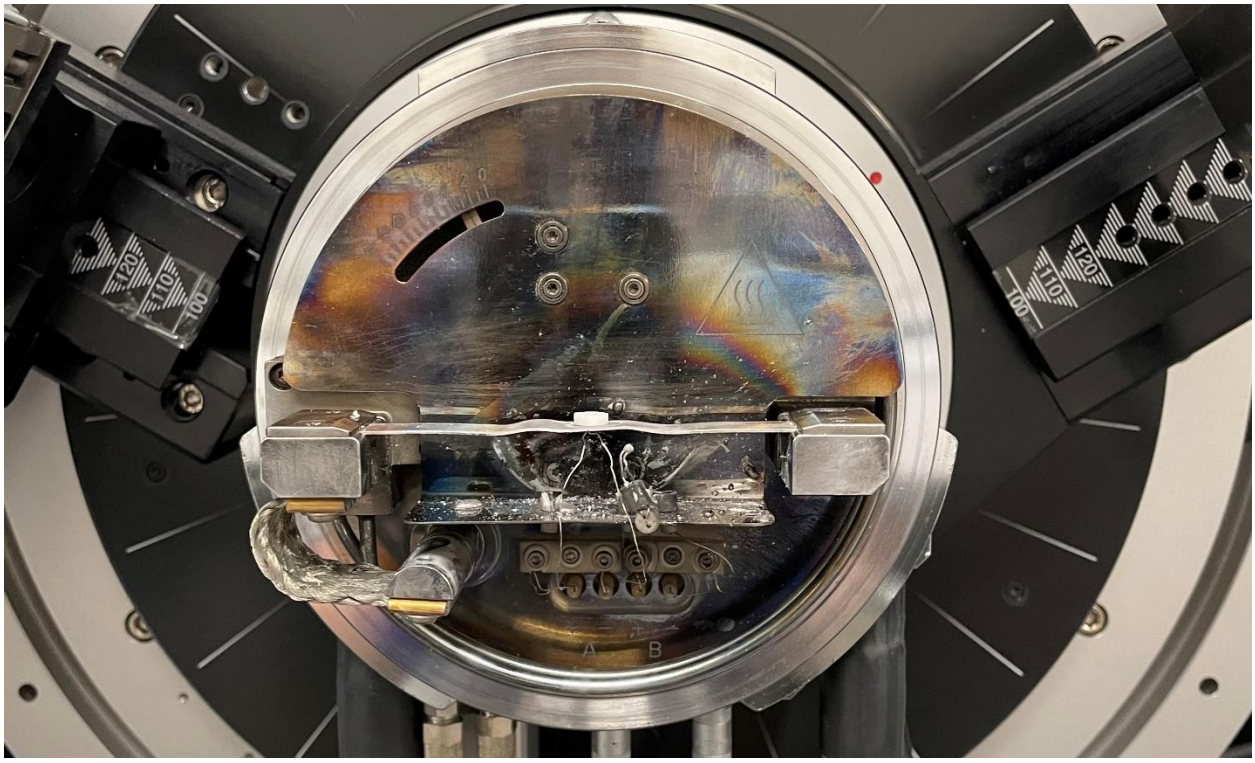

Figure 12: Hotstage sample holder installed with pellet in the center of the diffraction path.

The holder is a platinum plate that has two thermocouples welded to the bottom of the plate to heat the sample through resistive heating. The chamber is sealed, and the diffraction beam passes through a thin layer of Kapton tape. The chamber has a slight overpressure of helium to prevent flow of ambient atmosphere from penetrating the Kapton as it is permeable. The sample is scanned several times at room temperature to

determine the height of the sample to properly adjust the diffractometer. If the beam is not level with the sample the scan could fail, cause significant shifts in peaks, or only detect the platinum stage.

4.4.2 Operation

Salts were packed and leveled into 25 mm diameter polymethyl methacrylate sample holders. An auto sample holder is attached to the XRD that can fit up to nine samples (**Figure 13**).

Figure 13: Multiple samples loaded into the ambient sample holder for the XRD.

A standard sample scan produces a measurement at a step rate of 0.015 2-theta/scan. Depending on the range of interest for 2-theta the scan can take upwards of two-hours. A slow step rate produces a higher resolution scan with sharp intense peaks.

The experimental parameters tabulated in **Table** 4 for the non-ambient sample chamber, or the hotstage, are dependent on the sample. This example uses pure $MgCl_2$ as an example for the temperature holds. Subsequent experiments were scanned below melting point and above the melting point, then once more at 30°C after being cooled down slowly in hopes that recrystallization has occurred with preferred orientation of the crystalline structure.

Table 4: Operating parameters for $MgCl_2$ in the hotstage

Operational Parameters	**Setting**
Temperature Holds	30, 700, 750°C
Ramp Rate Increasing	10°C/sec
Ramp Rate Decreasing	10°C/min
Gas Connection	Helium
Gas Flow	50 mL/min
Delay Before Scan	440 sec
Scan Speed	0.2 sec/step

Each temperature scan is roughly two hours long which can result in phase changes or peak shifts in the spectra due to the evolution of the sample at temperature.

CHAPTER 5: SODIUM POTASSIUM CHLORIDE

5.1 Introduction

The sodium potassium system has been studied thoroughly in the field of concentrated solar, but at the start of this work had not been well studied regarding the requirements for the nuclear field.[75, 76] Extensive studies in concentrated solar provided new methodologies for analysis of sodium-potassium chloride at elevated temperatures, however the temperatures analyzed were not as high as required for molten salt reactors. The data reported in literature at lower temperatures was used to verify new methodologies before tests begin at reactor operation temperatures ~100ºC above the melting point and greater. The sodium potassium chloride salt system was chosen as the benchmark system to develop thermophysical property methodologies and establish capabilities with confidence. The salt compositions were chosen to be evenly distributed along the phase diagram (**Figure 14**).

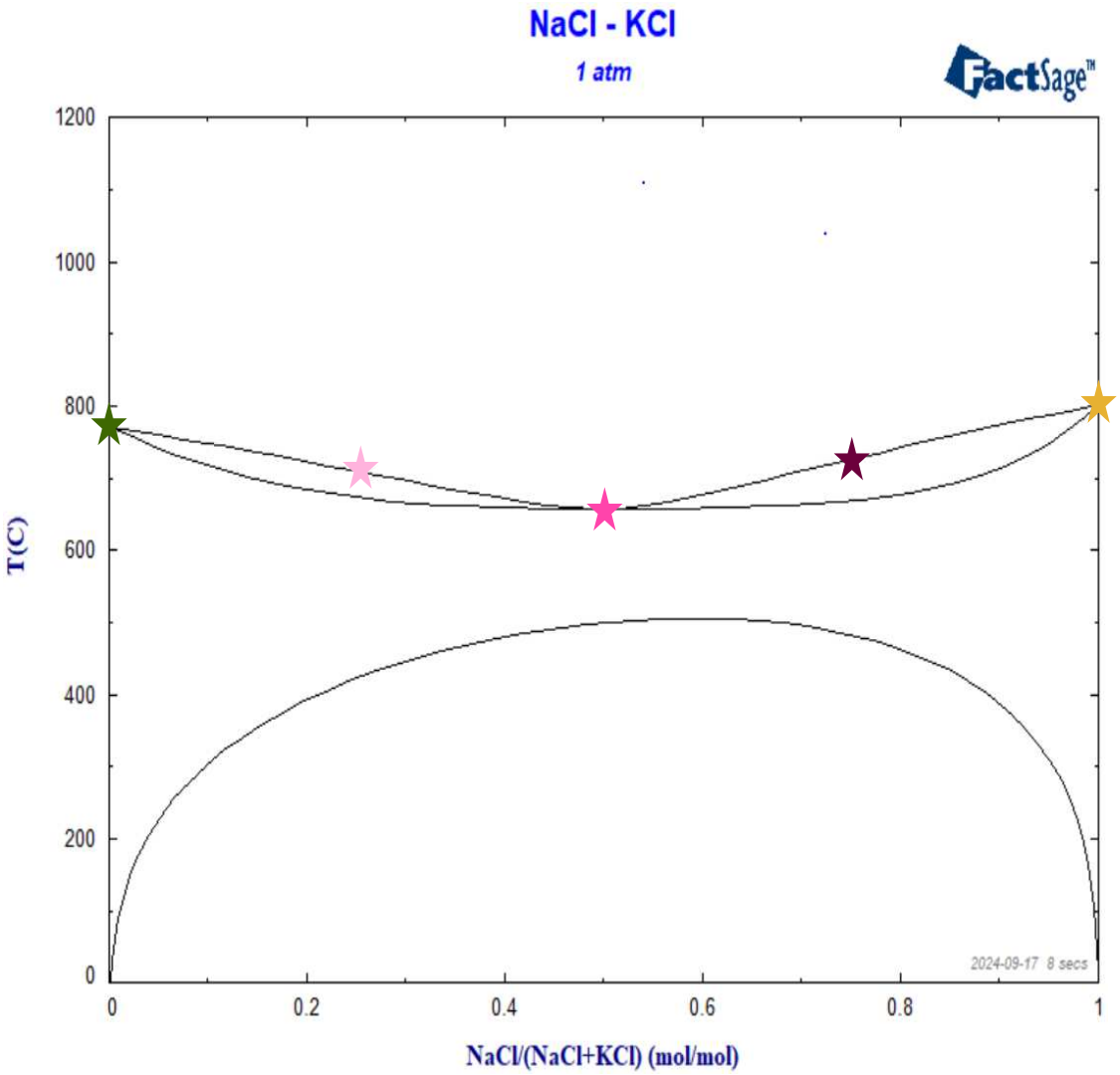

Figure 14: FactSage (Thermfact/CRCT, Montreal Canada and GTT-Technologies, Aachen, Germany) generated phase diagram of NaCl-KCl with stars representing compositions of interest. Pure endmembers, two midpoints, and the eutectic point.

The first capability to be established was HTDC to determine enthalpy and heat capacity. Density was next through several trial-and-error methods until a simple benchtop pycnometry method was determined to have good reproducibility with values comparable to the literature. Vapor pressure and volatility studies used a collection of analytical techniques and instrumentation to draw conclusions about the changes occurring in these complex systems as they go through intense heating and cooling. For the sodium

potassium chloride salts, TGA and EGA were used to understand the phenomenon of the gaseous release occurring at lower than predicted temperatures.

5.2 Batching

Source salt containers (Sigma-Aldrich, KCl, Anhydrous ACS Reagent ≥99%, Sigma-Aldrich, NaCl, Anhydrous ACS Reagent ≥99%) were stored in a nitrogen controlled inert glovebox to reduce atmospheric exposure. Some batched salt samples were left in open atmosphere to study the effects of humidity (water) exposure on the system. Humidity studies were not systematic, and the water content of the salts exposed to atmosphere was not identified. Batch calculations were performed depending on the molar percent of the given salt in the composition (**Table 5**). The nomenclature used in **Table 5** is relative to the molar percent of individual salts in the binary compositions. For example, a sodium-potassium chloride sample containing 100% NaCl is written as ClNaK10000; The eutectic composition containing 51 mol% NaCl and 49 mol% KCl is written as ClNaK5149.

Table 5: Ideal molar ratio for the sodium potassium chloride series

Sample ID	Batch (mol %)	Batch Total (g)	NaCl (g)	KCl (g)
ClNaK10000	100:00	5.0000	5.0000	0.0000
ClNaK7525	75:25	5.0000	3.5083	1.4917
ClNaK5149	51:49	5.0000	2.2466	2.7534
ClNaK2575	25:75	5.0000	1.0359	3.9641
ClNaK00100	00:100	5.0000	0.0000	5.0000

Salts were weighed, then combined and mixed using a mortar and pestle for five minutes before being stored in vials. The sample vials were kept in the glovebox and only the required masses of samples were removed from the vial to reduce atmospheric exposure during transport.

Depending on the instrument used, the salts were prepared in separate ways to be tested. Both chloride and fluoride salts are extremely corrosive in their liquid and gaseous forms at high temperatures. To prevent long term damage to instrumentation and reduce the amount of salt volatilization, the samples were held in alumina, aluminum, or nickel crucibles. Calorimetry samples were massed to 20-25 mg of salt and contained in aluminum and nickel crucibles. Samples were prepared in the glovebox and lids were pressed onto the crucible for safe transportation to the laser welder. The laser welder was used to seal the crucibles and protect instrumentation. For thermogravimetric experiments, roughly 11 mg of sample were contained in 150 µL alumina crucibles. Mass spectrometry experiments utilized a quartz tube to contain one gram of sample, the purpose of these experiments was to understand the volatilization and they therefore required an open containment. 10 mL cylindrical alumina crucibles packed with ~12 g of sample were used for the geometric pycnometry density methods.

5.3 Density

5.3.1 Methodology

The density procedure used to measure ClNaK was modified from methods and calculations in previous studies found in literature.[57] In previous studies pellets of salt were pressed to a known volume prior to the test. Pellets were next placed in a platinum crucible, held by a secondary crucible, and melted in a box furnace. The furnace was ramped from room temperature to the desired testing temperature at 10°C/min and then set to dwell at temperature for one to three hours depending on the sample. Severino's[57] assumptions were if the salt was allowed to overflow into the secondary containment

crucible of known volume, the primary crucible would then contain the full amount of salt at melting temperature. Any overflow that was not confined to the crucible during the melt is considered excess and not necessary for the calculation. Severino[57] accounts for the meniscus that forms and addressed the change in Equation 18, with the assumption that the meniscus is uniform and spherical in natural.

$$\rho_{MS}(T) = \frac{m_{total\ (T)} - m_{crucible}}{\frac{m_{H_2O}}{\rho_{H_2O}} \cdot \left(1 + \beta_{alumina} \cdot [T - T_{ambient}]\right) + \frac{1}{6}\pi h\left(3a^2 + h^2\right)} \quad \text{(Eq. 18)}$$

where ρ_{ms} is the density of the molten salt sample as a function of temperature, m is the mass, ρ_{H2O} is the density of water at room temperature, β is the thermal expansion coeffiencent for alumina, T is temperature, a is the radius of of the spherical meniscus, and h is the height of the meniscus. The assumption that the mensicus is spherical in nature is not an ideal approximation due to the true shape having conical sides and a flat surface when cooled.[57] However, if the salt was overflowing the crucible, there is no need to account for the meniscus height.

The modified procedure is experimentally the same. The empty crucible is weighed, and its dimensions measured with calipers five times to achieve a precise measurement. For these experiments high-purity alumina crucibles were used in two sizes, a short-stout cylindrical crucible (crucible A), and a tall, narrow cylindrical crucible (crucible B) (**Table 6, 7).**

Table 6: Initial measurements of crucible A.

Measurement	Inner Diameter (cm)	Radius (cm)	Inner Height (cm)	Empty Mass (g)	Volume (cm^3)
First	2.137	1.069	2.419	19.8324	8.672
Second	2.182	1.091	2.428	19.8320	9.075
Third	2.142	1.071	2.459	19.8327	8.857
Fourth	2.116	1.058	2.466	19.8325	8.668

Fifth	2.155	1.078	2.443	19.8328	8.906
Average	2.146	1.073	2.443	19.8325	8.835
St. Dev.	0.02	0.011	0.02	0.0003	0.2

Table 7: Initial measurements of crucible B.

Measurement	Inner Diameter (cm)	Radius (cm)	Inner Height (cm)	Empty Mass (g)	Volume (cm^3)
First	1.791	0.896	3.215	21.8328	8.095
Second	1.824	0.912	3.186	21.8329	8.321
Third	1.805	0.903	3.189	21.8329	8.156
Fourth	1.802	0.901	3.193	21.8330	8.139
Fifth	1.793	0.897	3.185	21.8329	8.038
Average	1.803	0.902	3.194	21.8329	8.150
St. Dev.	0.01	0.006	0.01	0.0001	0.1

Once initial measurements were taken, the salt powder was fully packed into the crucible, which ranged from nine to thirteen grams of sample, and placed in an overflow crucible to preserve the furnace (**Figure 15**).

Figure 15: Fully packed crucible in overflow container.

The furnace was programmed with a ramp rate of 10°C/min until the target temperature was reached. The furnace then maintained an isothermal hold for two hours to ensure a

uniform melt was achieved. After the two-hour isothermal hold the furnace was shut off to allow for a rapid cool and to minimize the production of vapors and additional mass loss. Once cooled, the crucibles were wiped of any excess salt that overflowed and weighed. The starting volume was divided by the final mass to determine the density of the salt at the target temperature. The initial inner volume was used for the modified calculation. The calculation has been simplified to mass at melt over volume of crucible in Equation 19.

$$\rho = \frac{m_f}{V_i} \qquad \text{(Eq. 19)}$$

5.3.2 Results and Discussion

Experiments were conducted at target temperatures from 700-1000°C in triplicate at every target temperature for each of the ClNaK compositions. **Figure 16** shows the change in density with change in temperatures compared to literature value.

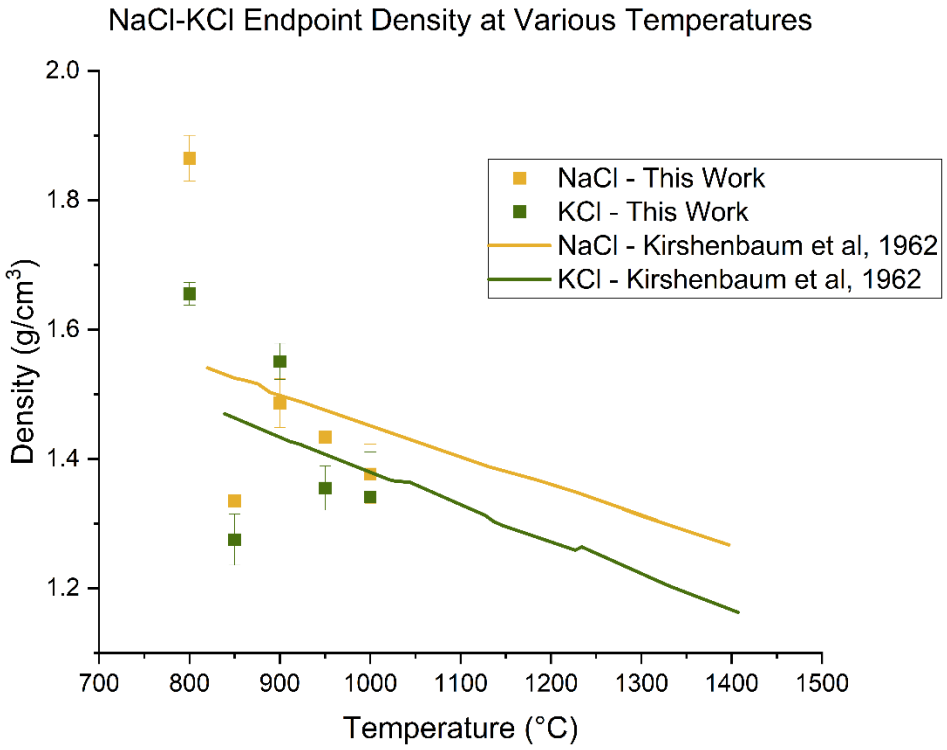

Figure 16: The density of the pure NaCl and KCl plotted with literature values, uncertainty is two sigma.

Sodium chloride has a melting point of 801°C causing the data point at 800°C to measure between the solid phase density of 2.16 g/cm^3 and partly in the liquid phase. This result also addresses the assumption that the sample had come to a complete melt during the experiment. A complete melt can be verified visually as a fully melted and cooled sample will have a glassy appearance. In the case of ClNaK10000 at 800°C, the sample still had visible powders. Potassium chloride has a melting point of 770°C, and the measured density was much higher than literature values. The melting point discrepancy for potassium chloride could be caused by impurities in the salt from the vendor, temperature variance in the furnace, or from high vapor pressure.

The same experiments were conducted with the midpoint and eutectic point compositions (**Figure 17**).

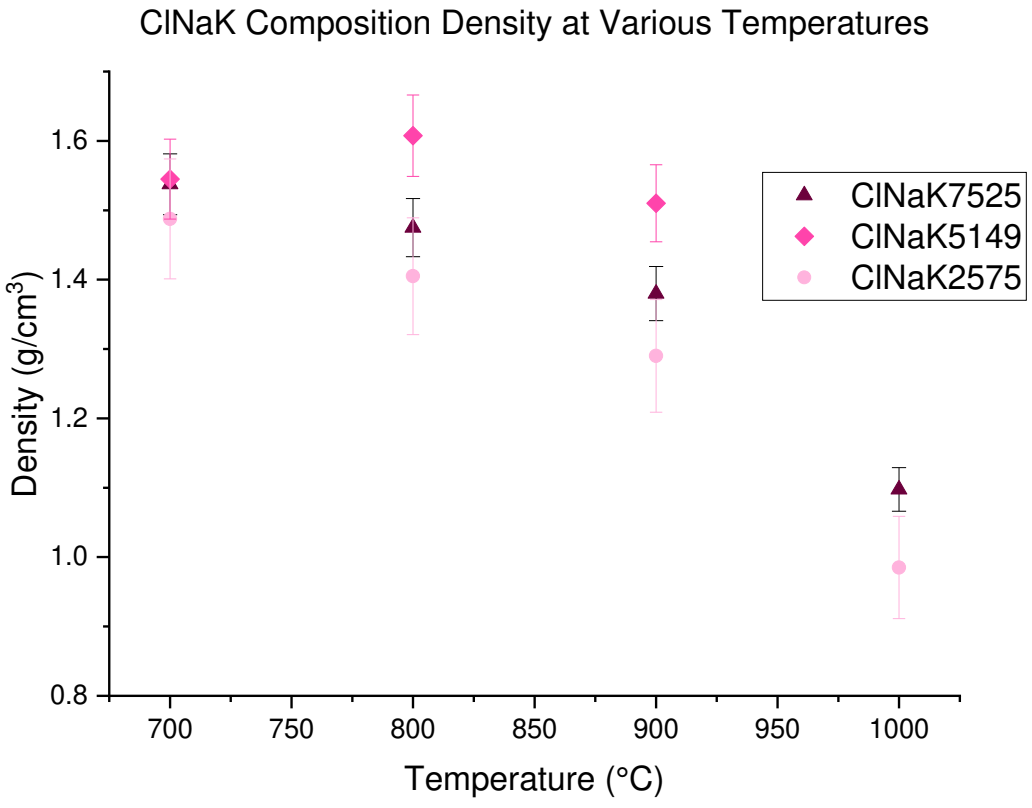

Figure 17: Experimental density values for mixed compositions of ClNaK, uncertainty is two sigma.

The midpoint compositions follow the fundamental trend of decreasing in density as more components are mixed into the salt composition. The ClNaK7525 midpoint has a higher density than the ClNaK2575 midpoint composition which follows the trend that pure NaCl has a higher density than KCl. There appears to be a significant decrease in density by 1000°C which may be caused by the rapid vaporization at increased temperatures. The eutectic composition had higher measured density than both midpoint compositions. One important caveat to this method is that it assumes no amount of sample is lost by volatilization. However, one hypothesis to explain this observation is that volatility of ClNaK is not congruent.

Severino[57] had many assumptions associated with the experiment, some of which carry over to the modified tests. One assumption is the porosity and thermal expansion of the crucible is negligible; however, over time the crucible degraded which proves the salt was seeping into and/or corroding the crucible. As the crucible was reused during the experiment and remeasured there was a slight expansion. This led to the speculation that the salt forced a more extreme thermal expansion by seeping into micropores in the crucible and recrystallizing or combining with the material. To reduce the effects of this, salt was packed into the crucible and brought to a target temperature and allowed to melt completely and fully mix, seep and recrystallize into the crucible. The first measurable trial used the crucible and recrystallized salt from the previous trial and then packed to the top again with fresh salt. This ensures that overflow occurs, and the meniscus only forms upon cooling. The overflow also eliminates the assumption of creep from the salt during cooling. The final assumption that remains is no volatilization of the salt. There is

clear evidence that the salt is volatilizing based on mass loss during the trial. The samples' volatilization rate is unknown, but with progress being made on vapor pressure and volatility experiments, a correction factor could be applied to these measurements and subsequent thermal measurements in the future.

5.4 Enthalpy and Heat Capacity

5.4.1 Materials and Methods

A Calvet DC Alexsys (Setaram, KEP Technologies, France) high temperature drop calorimeter was used to ascertain heat capacity and enthalpy data. For NaCl-KCl and to establish the capability, many crucibles were tested to see which would withstand the temperature and corrosive nature of the salts while maintaining full containment. Aluminum, silver, nickel, and molybdenum alloys were tested at different sizes. The geometry of various designs was also tested, e.g., a crimped toothpaste tube style crucible and a pill capsule type. The final design was a custom fabricated nickel crucible (~150 µL) with a tapered lid that can be press fit and sealed in an inert atmosphere for a safe and contained transport (**Figure 18**).

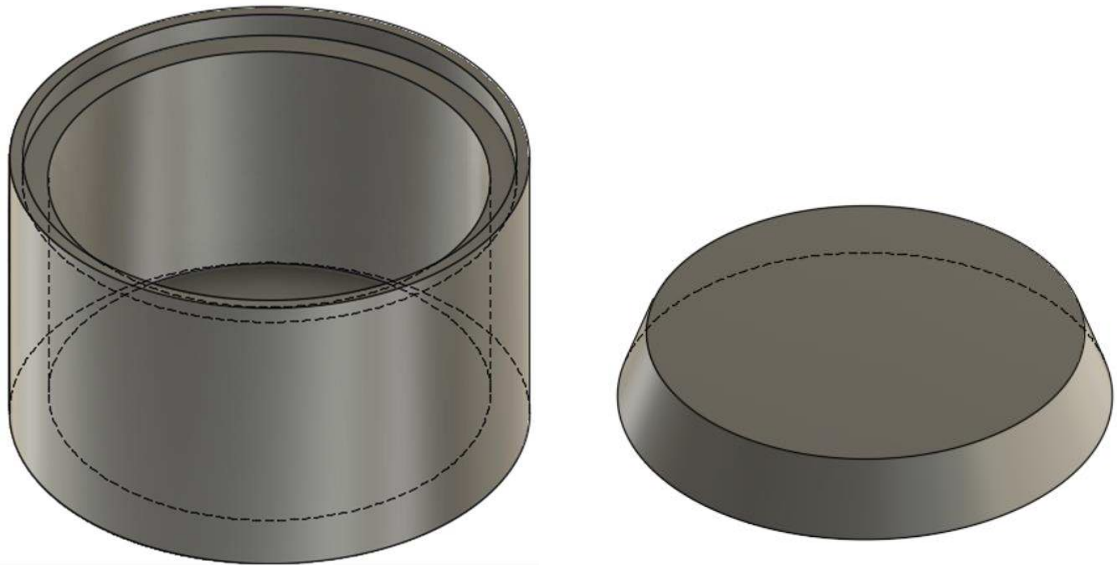

Figure 18: CAD drawing of the fabricated nickel crucible.

The crucibles were prepared with roughly 20 mg of sample before being press fit to transport to the laser welder to be sealed. Either in continuous or manual firing of the laser, the welding is done by manually moving the sample and overlapping the welds. Precise welds take experience, and it was observed that discrepancies can be introduced between each weld and between individuals. Samples are weighed in three stages in triplicate to ascertain any material loss during the welding process. Mass is determined of the empty pan and lid, then with the sample, and after welding on the lid. Typically, there is a small loss of mass 1-2 mg that can be associated with nickel material being ablated during the welding process. The samples must be sealed to withstand the insertion into the instrument and ensure no contents leakage of the molten salt and endure additional pressure changes within the capsule.

The HTDC is set to the target temperature 24-48 hours prior to use for the thermal control zones to reach an equilibrium. A detailed description of the workflow used for analysis via HTDC is given in Chapter four, but to summarize: an initial baseline experiment is

conducted with empty tubes and run for approximately the length that a normal experiment would be conducted, eight hours. The baseline needs to be achieved prior to the next drop for consistent determination of the area under the curve. Once the baseline is collected, empty crucibles are dropped to establish the background of the nickel crucibles to be averaged and subtracted from the measurements containing samples. The samples are then dropped, and the resulting drop curves are integrated to collect the total signals from the individual samples.

5.4.2 Results and Discussion

The literature values from Pan[77] were used to verify the methodology by comparison of heat capacity values. Pan[77] reported both simulated and experimental values for NaCl and KCl. The simulated value for KCl was reported as 70.30 kJ/mol·K, and the experimental value was 67.00 kJ/mol·K. The simulated value for NaCl was reported as 68.2 kJ/mol·K and an experimental value of 67.0 kJ/mol·K was determined. The experimental and simulated results were quite similar, with KCl being marginally higher than sodium chloride. **Figure 19** shows the plotted experimental values calculated using the equations described in Chapter four, with the slope of the line representing heat capacity (**Table 8**).

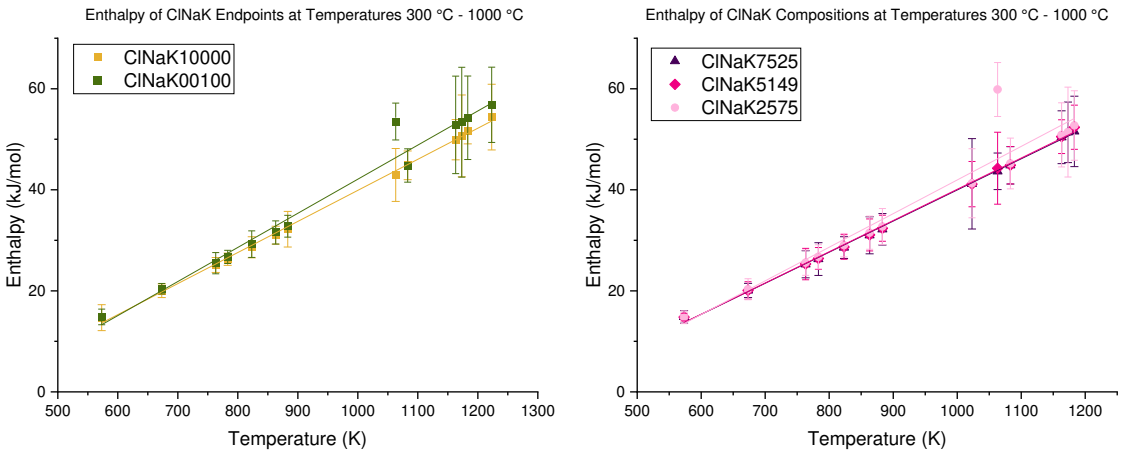

Figure 19: Calculate and plotted enthalpy values for the ClNaK system, uncertainty is two sigma.

Table 8: Line equations corresponding to the plotted values in Figure 19.

ClNaK	Slope (kJ/mol·K)	Intercept	Heat Capacity (J/mol·K)
10000	0.06152	-21.4636	61.52
7525	0.06155	-21.5778	61.55
5149	0.06184	-21.7362	61.84
2575	0.06654	-24.5979	66.54
00100	0.06752	-25.4239	67.52

Heat Capacity is defined as the amount of heat necessary to change the samples' temperature by one degree. The trend is relatively the same as that of enthalpy, apart from temperatures higher than the melting point. Past the melting point for each composition, the heat capacity begins to decrease as the sample enters the liquid phase and lattice bonds begin to break. KCl and NaCl have the same lattice which could explain the closeness in values, but the NaCl has a slightly higher lattice energy due to the smaller atomic radii. Compositions with higher potassium chloride concentrations were determined to have a higher heat capacity and enthalpy than sodium chloride. One explanation could be possible phase changes or a change in the lattice during the heating

profile. As temperature increases so does the energy within the system, leading to the higher enthalpy values, ideally, regardless of the chemical composition.

5.5 Vapor Pressure and Volatility

5.5.1 Thermogravimetric Analysis

The thermogravimetric analysis technique utilized a TA Instruments SDT Q600 (Waters Corp, New Castle, DE) to determine rate of vaporization and vapor pressure at target temperatures of 700, 750, 800, and 900°C. Empty 90 µL alumina crucibles fitted with an alumina lid containing a small hole were used to tare the instrument. The sample pan was then removed, and the empty value was recorded prior to adding the salt sample. Once the sample was added the mass was recorded once more before adding the sample pan into the instrument. The operating parameters for the experiment are outlined in **Table 9**.

Table 9: Operating parameters and settings for the thermogravimetric analyzer.

Operational Parameters	Setting
Temperature Range	30°C to 900°C
Ramp Rate	Jump to target temperature
Gas Connection	Nitrogen
Gas Flow	50 mL/min
Isothermal Hold	1 hour
Pan Type	Alumina
Sampling Intervals	0.5 sec/point

5.5.2 Results and Discussion

Unfortunately, the instrument used became inoperative and was deemed irreparable during the trial and the experiments beyond preliminary results were not possible. The Antoine equation described in Chapter four was used to determine the k values at each temperature, as illustrated in **Figure 20**.

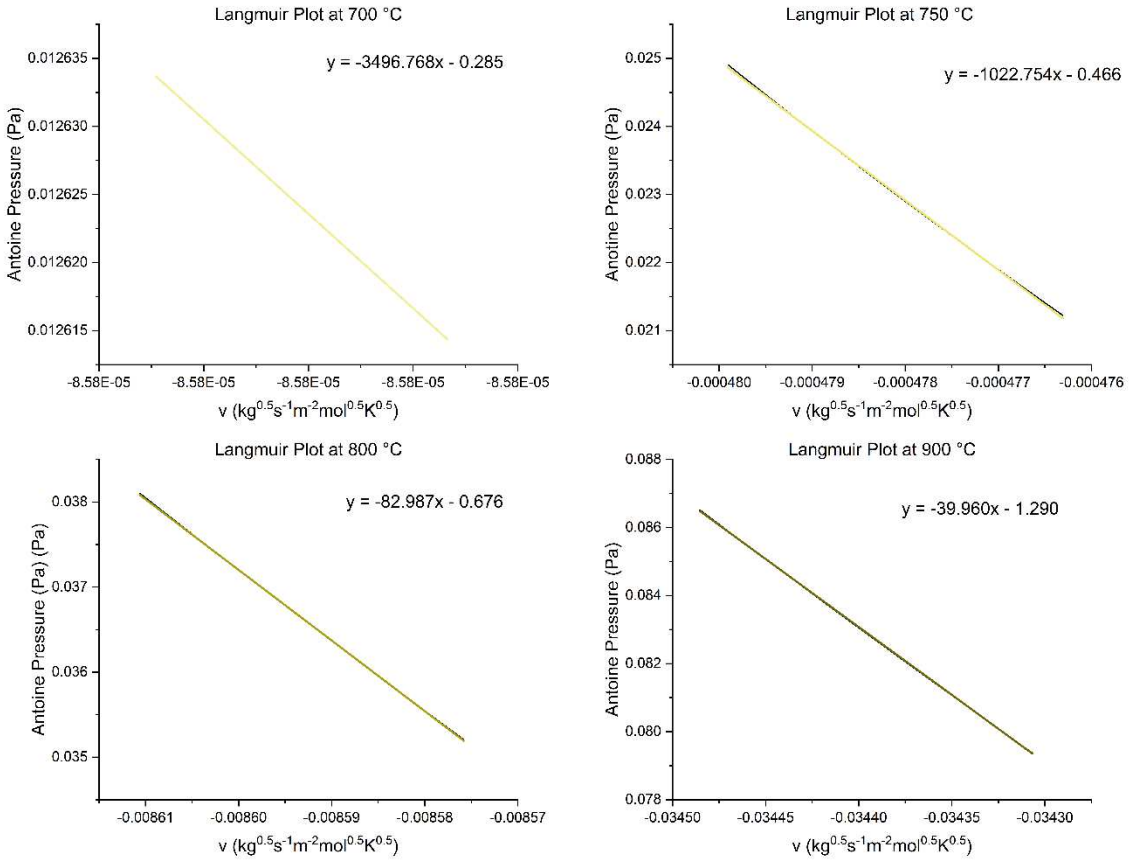

Figure 20: Vapor pressure calculated for temperatures of 700-900°C for ClNaK10000.

The k values at the tested temperatures were then used to calculate the experimental vapor pressure.

With increasing temperatures, a clear trend of increasing vapor pressure can be seen with a subtle drop in the pressure throughout the experiment as mass is lost within the system. ClNaK10000 samples were run under identical conditions and isothermal lengths; however, as temperature increases the sample would rapidly lose mass prior to the end of the experiment and eventually the crucible would be completely empty of sample. The amount of sample volatilizing can be seen in **Figure 21**, with a slope indicating potential rate of vaporization for that target temperature.

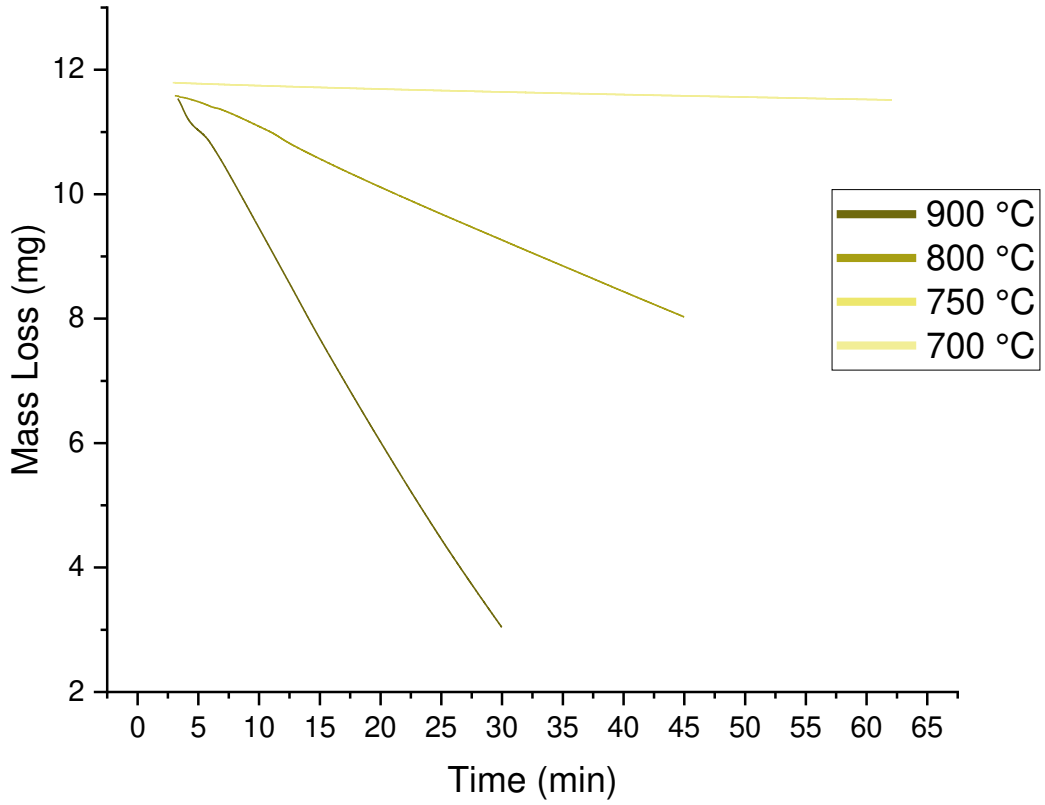

Figure 21: Mass loss over time during TGA experiments for ClNaK10000.

With better defined experiments and operating parameters, the determined rate of volatilization for each salt composition could be used as correction factor for other thermophysical property tests and correlate to operating parameters of other experiments.

5.5.3 Evolved Gas Analysis

A high purity quartz tube (30 × 2.5 cm) was weighed, and one gram of sample was then added to the tube and the total weight was measured. The tube was then placed in a custom designed muffle furnace and flushed with an overflow of argon gas. Once the gas flow had stabilized, the furnace was energized and a ramp rate of 10ºC/min was set until

the target temperature of 950°C was reached, followed by an hour-long isothermal hold (**Table 10**).

Table 10: Operating parameters set for the EGA during the ClNaK5149 experiment.

Operational Parameters	Setting
Isothermal Hold	950°C
Ramp Rate	10°C/min
Gas Connection	Nitrogen
Gas Flow	50 mL/min
Isothermal Hold	1 hour
Sample Holder	quartz tube
Sampling Interval	22 s/scan

To capture if the two salt components melted and volatilized congruently, mass numbers of sodium and potassium ions were input as scanning parameters in the MASsoft 10 Hiden Analytic Software (Hiden Analytical Ltd., Warrington, U.K.) as well as sodium chloride and potassium chloride (**Table 11**).

Table 11: List of mass numbers to be detected during the ClNaK5149 experiment.

Element/Compound	Mass Number
Water	18
Argon	40
Sodium	12
Nitrogen	28
Chlorine	35
Potassium	39
Sodium Chloride	58
Chlorine Gas	70
Potassium Chloride	74

5.5.4 Results and Discussion

In this study, the aim was to determine how the eutectic composition, CNaK5149, of volatilize using EGA-MS. The results show that in ClNaK5149, NaCl is releasing well

before the melting temperature as well as being the only species being released from the system. The results illustrated in **Figure 22** are from the same test displayed on different abscissa.

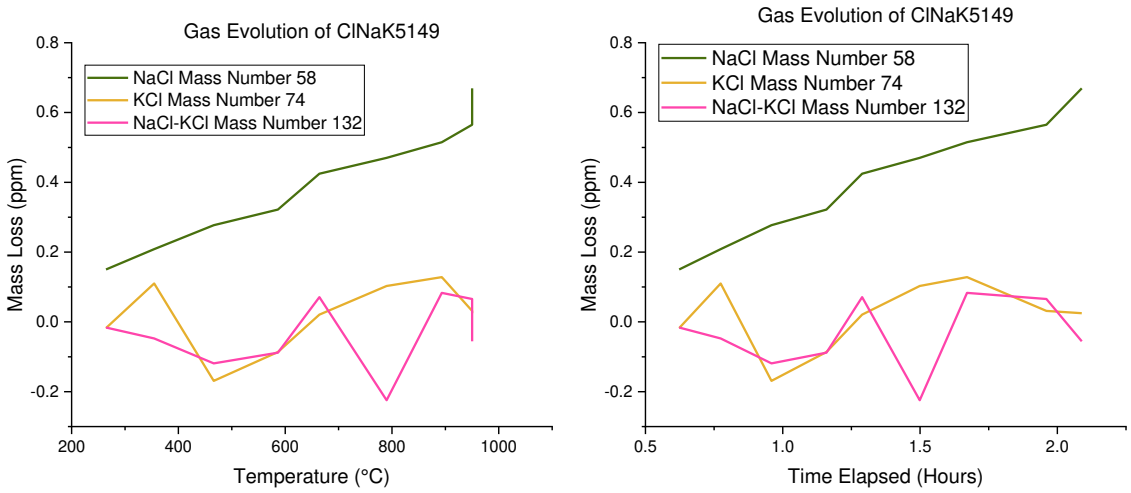

Figure 22: mass loss in ppm of specific mass numbers for the ClNaK5149 system.

The below zero results of the data for NaCl-KCl and KCl ions can be contributed to instrumental noise and reaching the limit of detection for the instrument (**Figure 22**). The incongruent release of NaCl to KCl could have a large significance in terms of measured thermophysical properties. If NaCl is volatilizing from the system before the salt melts and continues to volatilize at a higher rate than other compounds, the resulting reduction in NaCl contents would affect the composition of the salt system as a whole. The possible reduction of NaCl in the salt system due to volatilization may result in changes to the salt system and reduction in reactor efficiency, and possible effects on neutron economy. In addition, the volatilization of NaCl from the salt system could become a crucial concern in fuel salts if the stoichiometry of the system shifted sufficiently to precipitate solid actinide particulates out of solution.

5.6 Conclusions

Within the NaCl-KCl salt system, the eutectic composition appears to be less ideal as a coolant salt when vapor pressure and volatility behavior at elevated temperatures are considered. However, based on the enthalpy and heat capacity, a composition higher in potassium will function better for reactor operation as it will be more stable as a heat exchanger. Another considered qualification is that the densities of midpoints are relatively close together, which may be ideal for mixing of the salt during reactor operation. More work is needed to better understand the true nature of vapor pressure and volatility as these are likely to have the greatest effect on all other thermophysical properties. NaCl is preferentially released from the salt system well before the melting temperature of the eutectic composition. NaCl volatilization may have dramatic effects on the predictable function of the reactor. For example, this will change the fluid hydraulic conditions, density will change over time, and the heat capacity of the salt will be lowered. Due to these effects, it is vital that NaCl and other salt volatility is well understood for any of the ClNaK compositions to be used in a reactor.

5.7 Future Work

Though the sodium potassium chloride system was chosen as the benchmark for capability development due to previous work and references, there is still much to be done for this system. For example, higher resolution specific enthalpy and heat capacity data are needed in the temperature range of interest to molten salt reactors (e.g., 25-50°C increments between 300-1000°C). Thermogravimetric analysis measurements will need to be conducted in triplicate to verify the replicability of the measurement and a calibration method will need to be established. Various parameters and changes to the

systems should be tested as well. One parameter that could be adjusted is the carrier gas flow to the instrument. Carrier gas experiments should be run with as little overflow as 10 mL/min – 150 mL/min to determine how flow plays a factor in mass loss. Other carrier gas experiments could measure the salt just under the melting temperature to verify if the flow has an effect, or if the salt is being vaporized at temperatures while still being in the powder form. Different heating ramp rates could also be investigated with a focus on a jump (~10°C/s) to temperature to mimic HTDC experiments and a 10°C/min ramp to mimic all density and EGA experiments. Using this information, a correction factor for the rate of volatilization can be applied to other thermophysical experiments. More experimentation will need to be conducted focusing on the composition of the salt pre- and post- temperature changes. Understanding the change of the salts' molar ratio will determine if the batched ratio is still the same after a heat treatment is performed such as in the evolved gas analysis. If the NaCl compound is volatilizing as a salt vapor, then the composition is no longer the ClNaK5149 ratio that was predetermined prior to the experiment. Verification of NaCl volatilization, and other volatizing compounds, can be tested using inductively-coupled plasma optical emission spectroscopy (ICP-OES), laser induced breakdown spectroscopy (LIBS), or x-ray diffraction. Confirmation of a change in the molar ratio of molten salt compounds will be crucial for reporting accurate data for specific compositions. Lastly, density experiments should also be conducted with smaller increments of temperature changes to create a spectrum of densities rather than testing four target temperatures.

CHAPTER 6: MAGNESIUM POTASSIUM CHLORIDE

6.1 Introduction

Magnesium potassium chloride (KMgCl) was selected study because this system has been found to have advantageous heat transfer and thermal storage capabilities.[78-81] The potassium-magnesium chloride system is well documented (**Figure 23**).

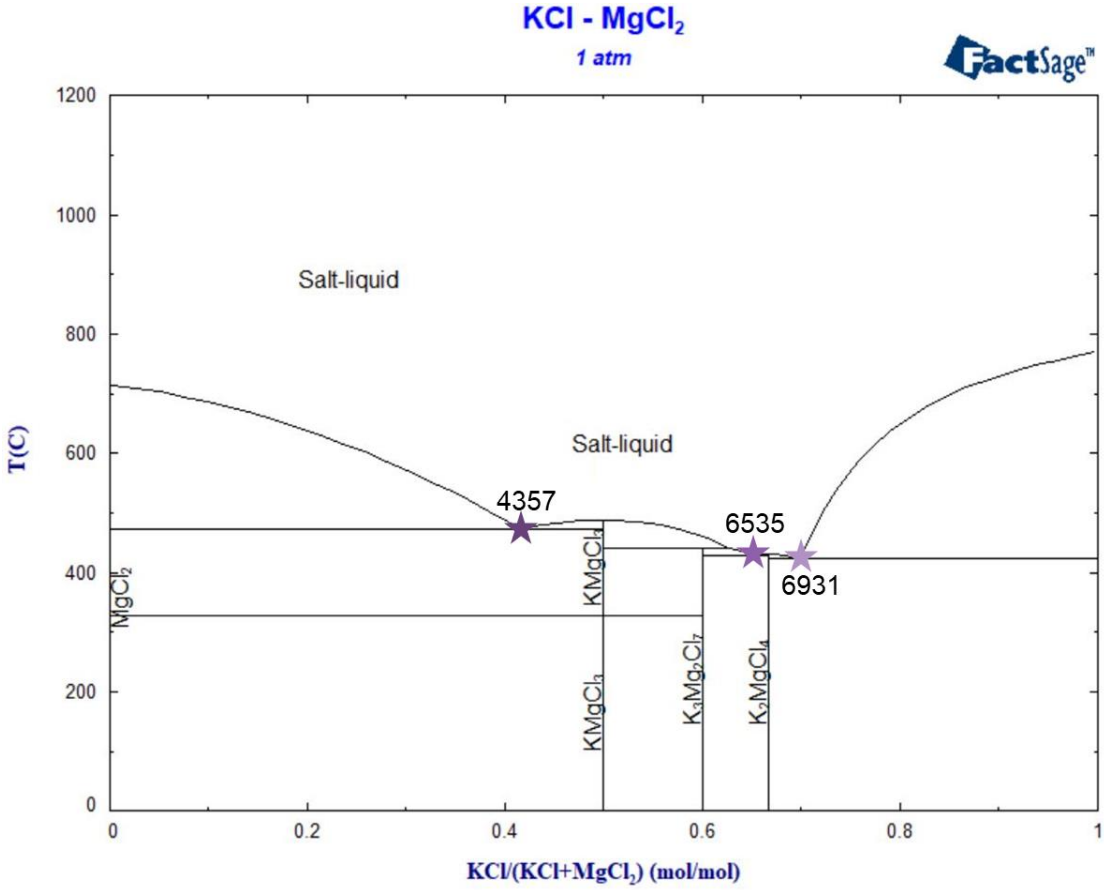

Figure 23: FactSage generated phase diagram of KCl-$MgCl_2$ highlighting phase changes and the eutectic points of interest.

The eutectic points were chosen because they have low melting temperatures, reportedly low vapor pressures, and have demonstrated excellent heat transfer properties.[81] KMgCl has data indicating good heat transfer properties; however, more in-depth studies on factors that could negatively impact the thermophysical properties are needed. One factor

is the effect of water content on proposed fuel and/or coolant salts' thermophysical properties. This chapter aims to highlight the differences between advertised as high-purity salt, assumed to be synthesized in inert atmospheres and sealed in inert atmospheres, and commercially available salts with advertised 99.99% purity, but not packaged, manufactured, or sealed in inert environments. If the thermophysical properties or chemical properties of proposed salt systems are negatively impacted with trace levels of water, salt for the reactor will require a purification process to ensure the salt matches all requirements to meet the thermal hydraulic calculations and no adverse effect or abnormality will occur. KMgCl enthalpy and heat capacity were determined using the HTDC method explained in previous chapters. Finally, various techniques were deployed to understand the vapor emanating from KMgCl at elevated temperatures. KMgCl emanation measurement techniques include XRD, non-ambient hot-stage XRD, and EGA.

6.2 Batching

6.2.1 Batching and Ratio Verification Materials and Methods

Commercially available, what will henceforth be referred to as 'off-the-shelf,' salts (Sigma-Aldrich, KCl, Anhydrous ACS Reagent ≥99%, Sigma-Aldrich, $MgCl_2$, Anhydrous ≥98%) were stored in a chemical cabinet whereas the ultra-dry salts (Sigma-Aldrich, KCl, AnhydroBeads™, −10 mesh, 99.9% trace metals basis, Sigma-Aldrich, $MgCl_2$, AnhydroBeads™, −10 mesh, 99.9% trace metals basis) were packaged in glass ampoules and sealed under argon, were opened in a nitrogen atmosphere glovebox. Three methods were used to batch the salt for this study: manually using a mortar and pestle for 10

minutes (ultra-dry and off-the-shelf salts), a tungsten grinder and puck in a shatterbox (off-the-shelf salts), and benchtop ball mill (ultra-dry salts). The compositions were batched based on the calculated molar ratio (**Table 12**).

Table 12: Calculated mass required for varying molar percent ratios of the potassium-magnesium chloride system, using five grams as an example.

Sample ID	Batch (mol %)	Batch Total (g)	KCl (g)	MgCl (g)
KMgCl10000	100:00	5.0000	5.0000	0.0000
KMgCl6931	69:31	5.0000	3.1771	1.8229
KMgCl6535	65:35	5.0000	2.9626	2.0374
KMgCl4357	43:57	5.0000	1.8567	3.1433
KMgCl00100	00:100	5.0000	0.0000	5.0000

The shatterbox allowed for a large amount of material to be batched at once and 150 g batches were produced, and all experiments were subsamples from the bulk source. The ball mill was used to combine the ultra-dry salt compositions in the glovebox. Combining the ultra-dry salts took several hours of mixing to achieve a uniform composition for each of the eutectic points. The material was first weighed and mixed manually with a mortar and pestle for 10-20 minutes. After manually mixing, the material was evenly distributed into the three ball mill vials. The vials, in total, could only hold approximately five grams of sample, so smaller batches were prepared for the ultra-dry samples. The ball-mill was then operated for an hour, then recombined manually before going back into the ball-mill. The ball-mill and manually mixing process was repeated three times. The sources of the ultra-dry compositions were then subsamples for HTDC crucibles.

To verify the ratios in each composition roughly one gram of each sample was pressed into a pellet for laser-induced breakdown spectroscopy (LIBS) analysis. A pulsed laser ablates a sample and creates a plasma that contains the excited electrons from the

sample. When the plasma begins to cools, the electrons start to relax emitting light that can be detected and displayed as specific spectral peaks related to the element or compounds.[82]

6.2.2 Ratio Verification Results and Discussion

Each sample was pressed into pellets in triplicate to assess the reproducibility of the batching method and then analyzed using LIBS. The calculated molar ratio was not achieved for salts prepared manually using a mortar and pestle as determined by LIBS. Additional mixing was required for manually mixed salts. The shatterbox method resulted in a uniform mixture that matched the calculated molar ratio, verified by LIBS. **Figure 24** shows the average value of the pellets that were pressed and the respective molar percent of the composition for both potassium and magnesium contents.

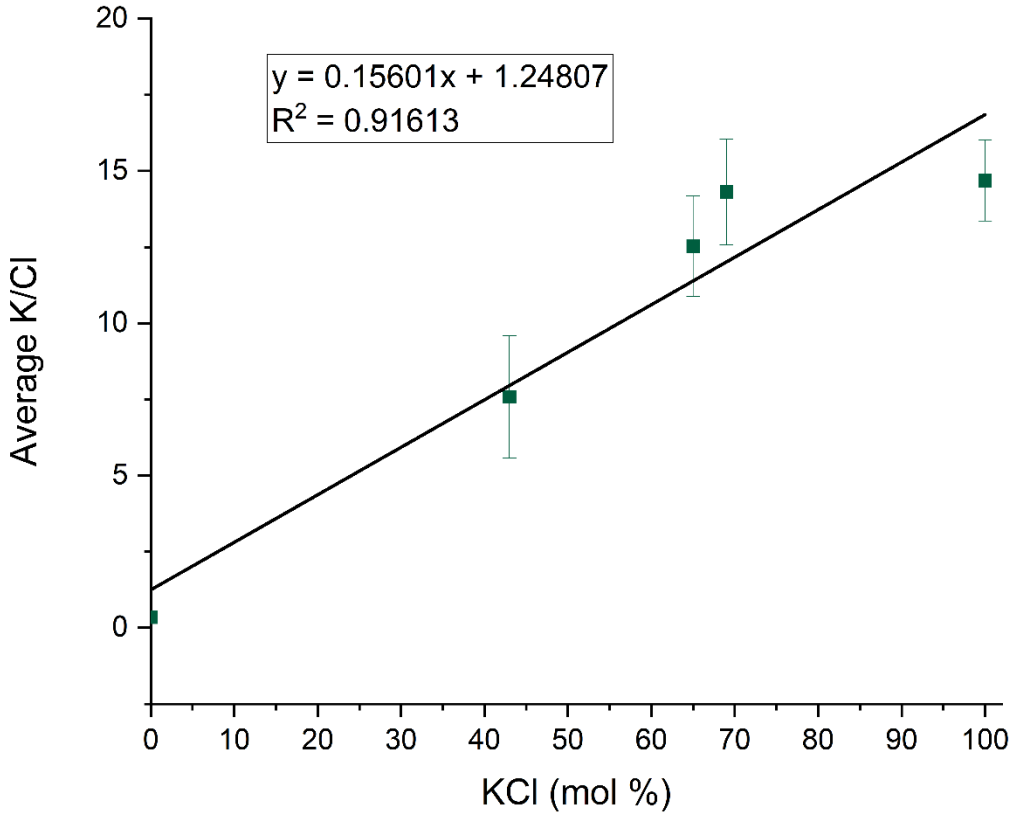

Figure 24: LIBS analysis of average batch ratio for KMgCl with shatterbox mixing, uncertainty is two sigma.

The plot shows that the batch is homogenous and that our subsampling approach is reproducible. This was then done with the ultra-dry salts producing the same similar results as present in **Figure 24**.

6.3 Volatility

6.3.1 Evolved Gas Analysis Methods

A high purity quartz tube (30 x 2.5 cm) was weighed and approximately two grams of sample added to the tube and the mass measured. The tube was then placed in the furnace and flushed with an overflow of argon or nitrogen gas depending on the

experiment. High purity nitrogen was primarily used when looking at any of the potassium containing salts as the low-mass peak tail of argon-40 interfered with potassium-39. Once the gas flow had stabilized and the sample was fully submerged in the inert atmosphere, the furnace was energized and a ramp rate of 10°C/min was set until the target temperature was achieved, and a 10-minute isothermal hold took place. The hold temperatures were 500, 600, 700, and 800°C (**Table 13**).

Table 13: Operating parameters and settings for evolved gas analysis.

Operational Parameters	Setting
Isothermal Hold	500, 600, 700, 800°C
Ramp Rate	10°C/min
Gas Connection	Nitrogen and Argon
Gas Flow	50 mL/min
Isothermal Hold	10 minutes
Sample Holder	quartz tube

Table 14 lists the ionization energies for the elements and compounds of interest, as well as the energy required to break apart the molecules.[83] Understanding the ionization and atomization energies aids in the optimization of operating parameters.

Table 14: List of first and second ionization energies for single elements and the atomization energy for KCl and $MgCl_2$.

Compounds	Ionization Energy I, II (eV)	Atomization Energy (eV)
Potassium (K)	4.34, 31.63	-
Magnesium (Mg)	7.65, 15.04	-
Chlorine (Cl)	12.96, 23.81	-
Potassium Chloride (KCl)	-	10.5
Magnesium Chloride ($MgCl_2$)	-	11.58

The mass numbers that were scanned are outlined in **Table 15**.

Table 15: List of mass numbers scanned during the KMgCl experiment.

Element/Compound	Mass Number
Water	18
Argon	40
Magnesium (II)	12
Oxygen	16
Magnesium (I)	24
Nitrogen	28
Chlorine	35
Chlorine	37
Potassium	39
Magnesium Chloride+	59
Chlorine Gas	70
Potassium Chloride	74
Potassium Magnesium Chloride	98

6.3.2 Evolved Gas Analysis Results

Off-the-shelf KMgCl6931 produced a chlorine spike at 300°C that occurred during ramping portion of the testing parameters rather than at the predicted isothermal hold (**Figure 25**).

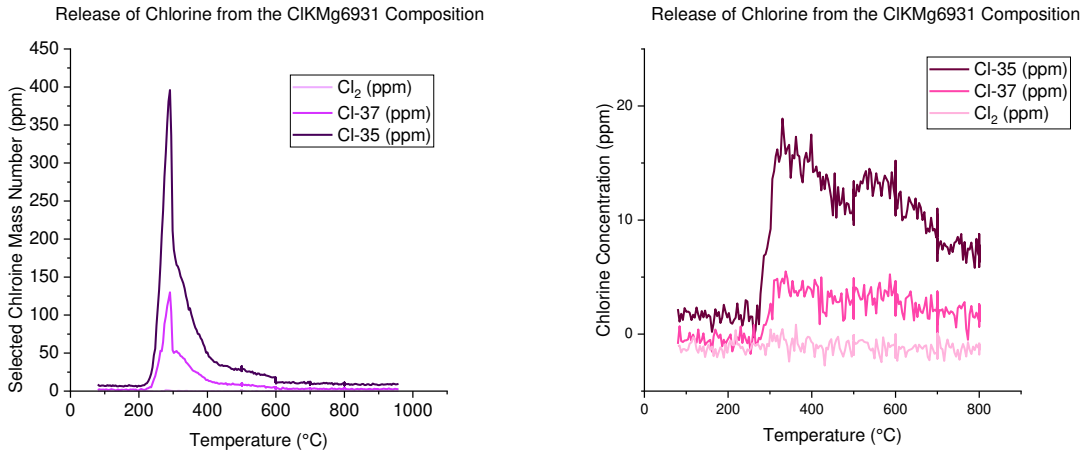

Figure 25: Selected chlorine mass number release from KMgCl6931 Left) KMgCl6931 ran in December sample taken from off-the-shelf salts. Right) KMgCl6931 ran in January taken from the ultra-dry batch prepared day of experiment in glovebox.

Off-the-shelf KMgCl6931 did not melt at the anticipated melting point ~423°C and was still in a solid phase past the melting point of KCl (770°C). The working hypothesis was the chlorine release allowed for an oxidation reaction to occur and convert the free magnesium into magnesium oxide. For this reaction to occur the following criteria for the chemical equation need to be met:

$$MgCl_2 + H_2O \rightarrow MgO + 2HCl \qquad \text{(Eq. 21)}$$

This led to the testing of the ultra-dry KMgCl0100 to determine if hydrochloric gas was being released alongside chlorine gas. **Figure 26** confirms the release of both hydrochloric and chlorine gas releasing at low temperatures during the ramping of the furnace which then allows for the conditions to be met to convert $MgCl_2$ to MgO.

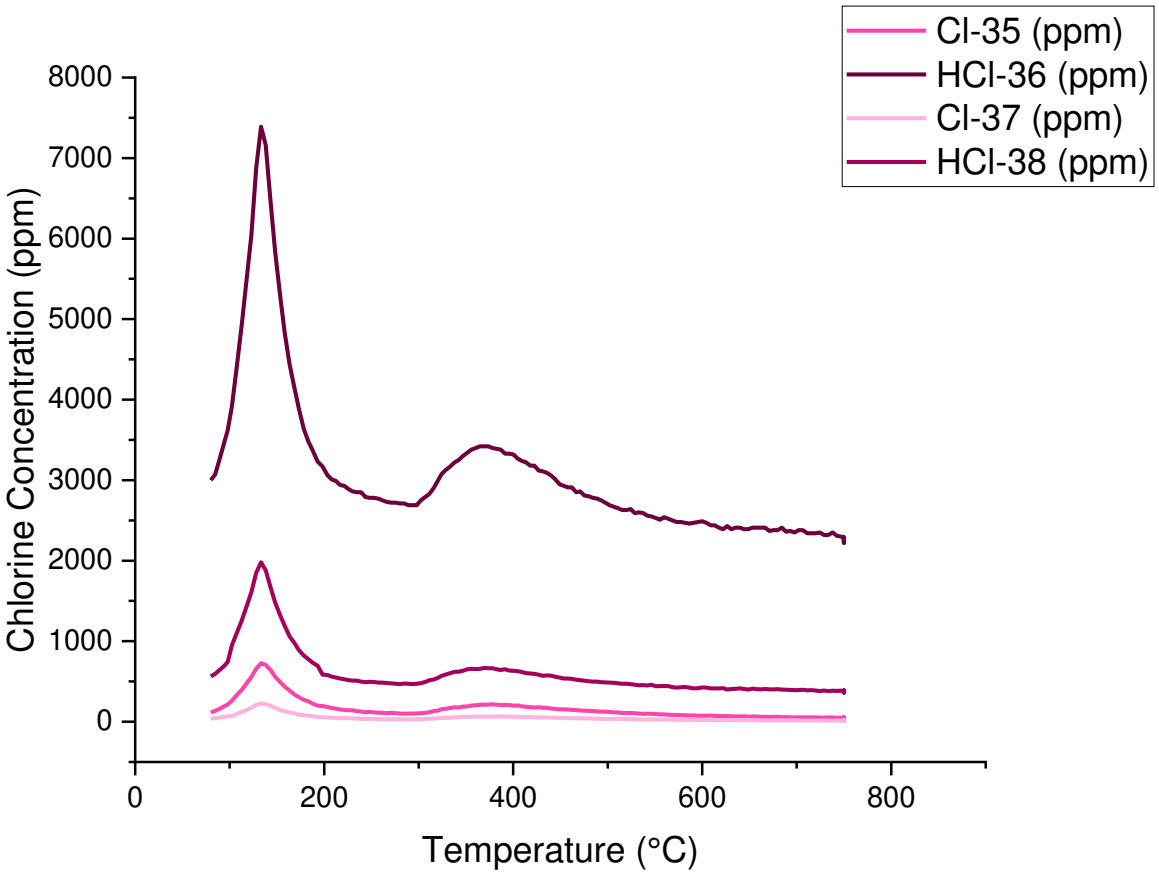

Figure 26: Selected chlorine mass numbers and hydrochloric acid mass numbers released from KMgCl0100.

To form $MgCl_2 \cdot 6H_2O$ an excess of water needs to be available, $MgCl_2$ (s) + $6H_2O$ (l) → $MgCl_2 \cdot 6H_2O$ (s), which at upon cooling could be absorbed during crystallization.

A major issue that was encountered during use of the EGA was plating of the salt in the unheated transfer line (**Figure 27**).

Figure 27: Recondensed salt on the air exposed quartz tube prior to reaching the heated capillary line.

The condensed salt forming on the quartz tube led to the assumption that any vapors detected in the EGA are plating out prior to reaching the heated capillary line. Another hypothesis is that if any vapors did reach the capillary line, the heat along the line was too low and would cause the salt to condense to the metal and again prevent the vapor from reaching the detector. The EGA is not a closed or fully inert instrument, and has minor leaks in the press sealed glassware, so the instrument still detects atmospheric water and nitrogen. KMgCl is hygroscopic, so working with an open system can influence the speciation of the salt forms, which is seen with the MgO conversion. EGA experiments were successful with highlighting chlorine being released during the ramping of heat process and allowing conversion of MgO to occur for the off-the-shelf batch of salts.

6.3.3 X-ray Diffraction (ambient) Methods

To better understand the behavior observed in the initial EGA experiments, the salts were analyzed by XRD. The first salts that were scanned were the off-the-shelf batches which were so hygroscopic they formed a crust during the scans which can be seen in **Figure 28**.

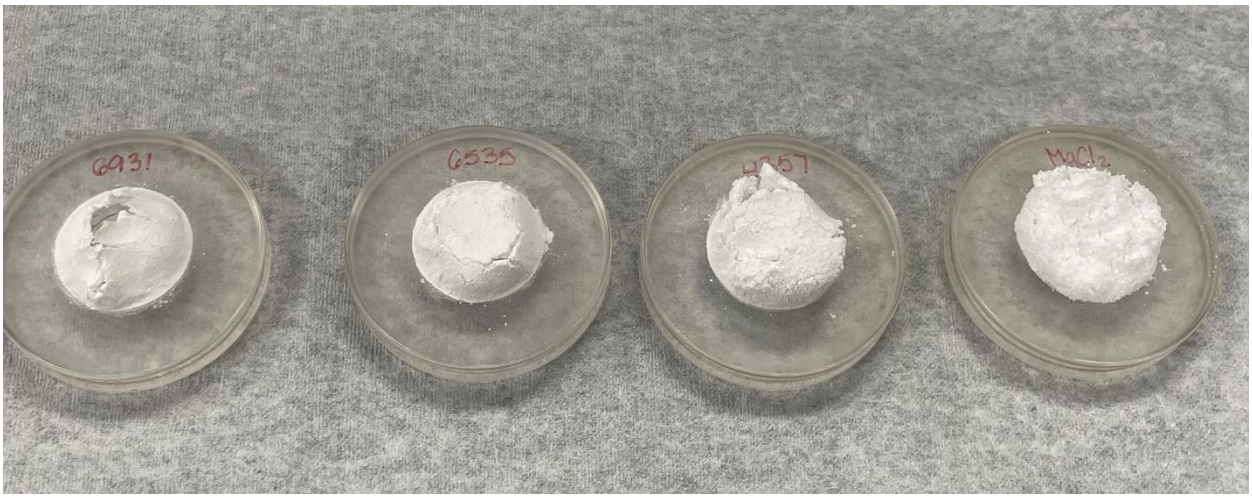

Figure 28: Samples after the XRD scan showing hydration and expansion.

The crust and resulting expansion prevented a successful analysis, likely because the beam was unable to be diffracted.as the surface was no longer flat and the beam pathway was impeded. Ultra-dry salts were also prepped and analyzed by XRD, also forming the crusted layer but at a much slower rate.

6.3.4 X-ray Diffraction (ambient) Results and Discussion

Two ultra-dry $MgCl_2$ samples, taken from the source container, were prepped inside the glovebox and one was transferred to the XRD and the other went to the EGA. The resulting spectrum from the sample immediately analyzed by XRD contained $MgCl_2 \cdot 6H_2O$ peaks. The peaks could be due to a trace impurity from the manufacturing process or water that was absorbed during the scan. The sample that was scanned after the EGA

experiment resulted in a less intense $MgCl_2$ peak than before the experiment. During EGA, is conducted within an inert environment, the conversion to MgO and further absorption of water occurred (**Figure 29**).

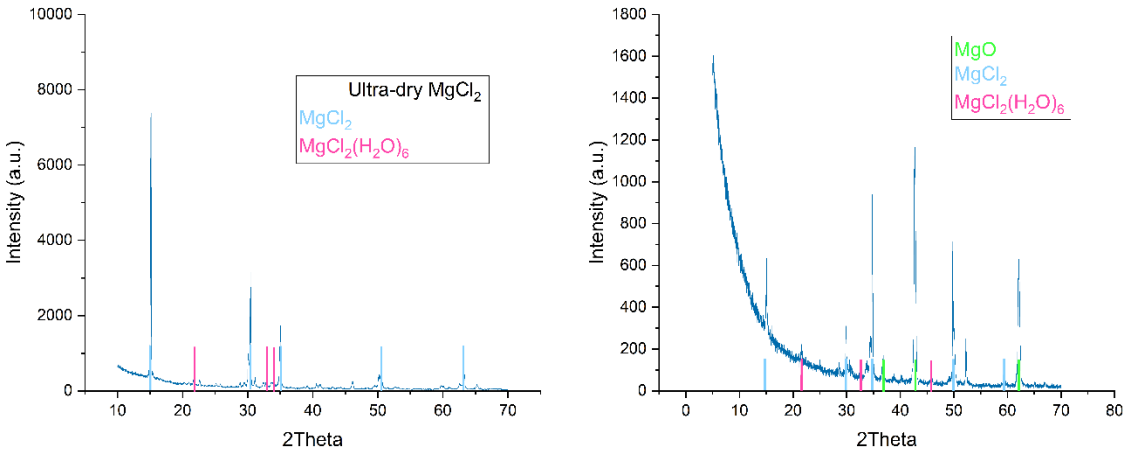

Figure 29: X-ray diffraction spectra of an ultra-dry KMgCl0100 sample. Right) prior to EGA experiment. Left) after EGA experiment.

Potassium chloride was determined to be the most abundant crystal in KMgCl6931 after being subjected to the EGA heating profile. (**Figure 30**).

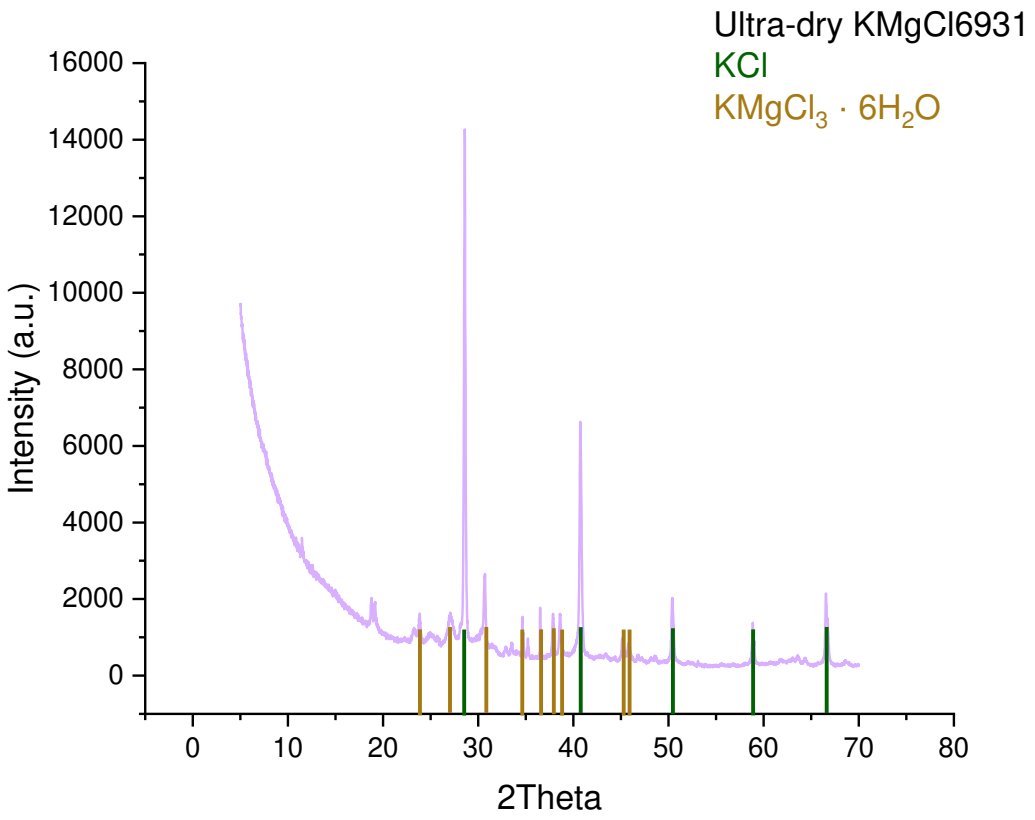

Figure 30: KMgCl6931 after EGA experiment with KCl and $KMgCl_3 \cdot 6H_2O$ peaks identified.

The resulting spectra contained no amounts of pure $MgCl_2$; however, $MgCl_2$ was present in the recombined composition, $KMgCl_2{\cdot}6H_2O$, giving evidence that upon cooling the salt recrystallizes as a uniform compound and absorbs water. The $KMgCl_2{\cdot}6H_2O$ peaks are present but not nearly as prominent as the KCl peaks. A hypothesis is that KCl is not fully mixing with $MgCl_2$ during melt and recrystallizes in concentrated areas as KCl. Another hypothesis is $MgCl_2$ is volatilizing during the melting process and the remainder of the salt is being recombined with KCl which addresses the less intense peaks of $KMgCl_2{\cdot}6H_2O$ and not having $MgCl_2$ peaks in the spectrum.

6.3.5 X-ray Diffraction (non-ambient) Materials and methods

The XRD non-ambient stage (hotstage) experiments were designed to understand the transition states salt will be subjected to upon heating with operating parameters previously outlined in Chapter four. To summarize, the scan of the starting material at room temperature captured the phases present and the baseline of those phases at the start of the experiment. Subsequent scans were taken at 50°C below the melting point, 50°C above the melting point, and the final one with a ramp down rate of 10°C/min. Ideally the final scan having a ramp down rate which allowed the salt to recrystallize in the preferred orientation and with mixed compositions. The ratio of phases present during the first scan could then be compared to subsequent scans to determine, for example, if MgO content increased throughout the experiment. Samples were pressed in small pellets to maximize sample recovery. Helium gas was supplied to the chamber and mineral oil bubbler to reduce the potential of backflowing water. The sample chamber is considered sealed; however, the detection windows are sealed with Kapton tape which is permeable. Thus, an overpressure of helium was supplied to the chamber to reduce the permeation of atmospheric gasses.

6.3.6 X-ray Diffraction (non-ambient) Results and Discussion

The hotstage was able to produce similar XRD spectra as the pre- and post-EGA spectra due to the ability of taking measurements at specific target temperatures that were outline in Chapter four. The peak at 40 2θ is from the platinum plate sample holder, this is most likely due to the beam path not being level with the sample stage. The platinum sample plate interference caused a slight shift in the peaks and the platinum to be detected (**Figure 31**).

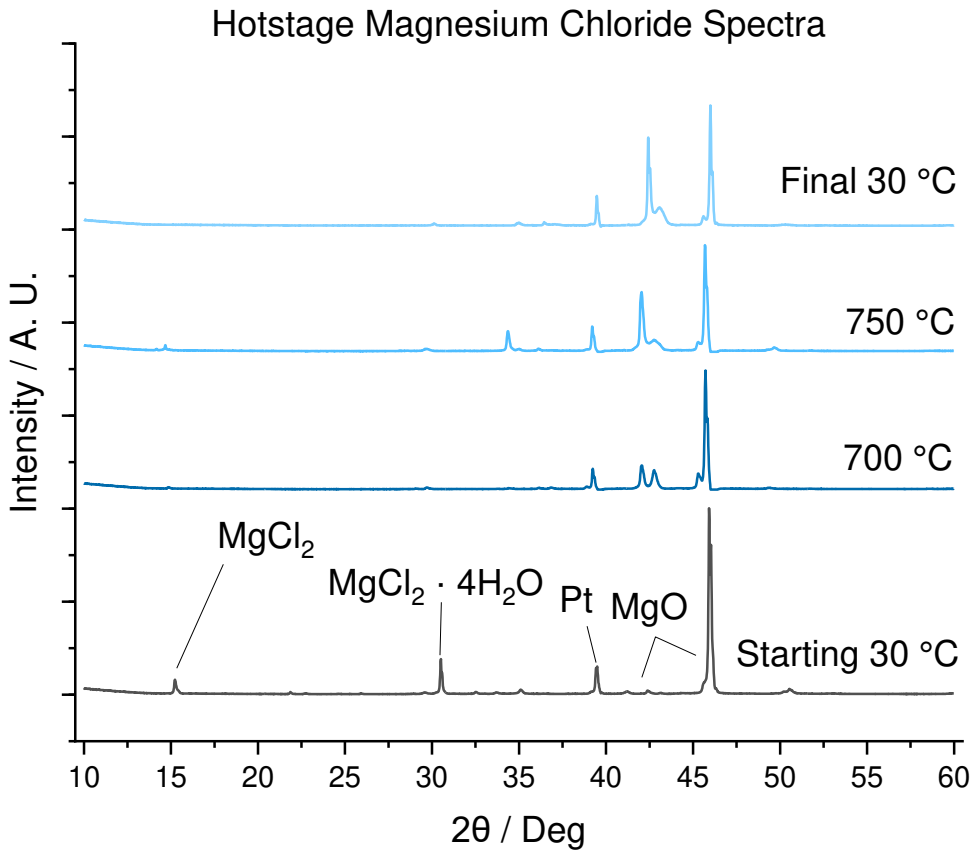

Figure 31: Hotstage XRD results of MgCl2 at target temperatures.

The pellet was pressed in the glovebox and then transferred with minimal exposure to the atmosphere before being placed on the sample holder and sealed in the chamber. The starting scan showed a large amount of MgO and $KMgCl_2{\cdot}4H_2O$ compared to $MgCl_2$. One explanation is the source material contained trace contaminants that are likely not evenly dispersed in the container. Another observation from the heated scans is that the $MgCl_2$ appears to fully convert to MgO, and the change is occurring prior to the melting point. The eutectic point, KMgCl4357 was chosen because it has the most even distribution of both endmembers with a slightly higher concentration of $MgCl_2$. This was to test if the $MgCl_2$ favored a reaction with KCl over the conversion to MgO. During the starting scan

at 30°C there are peaks indicating the presence of Magnesium and potassium (**Figure 32**).

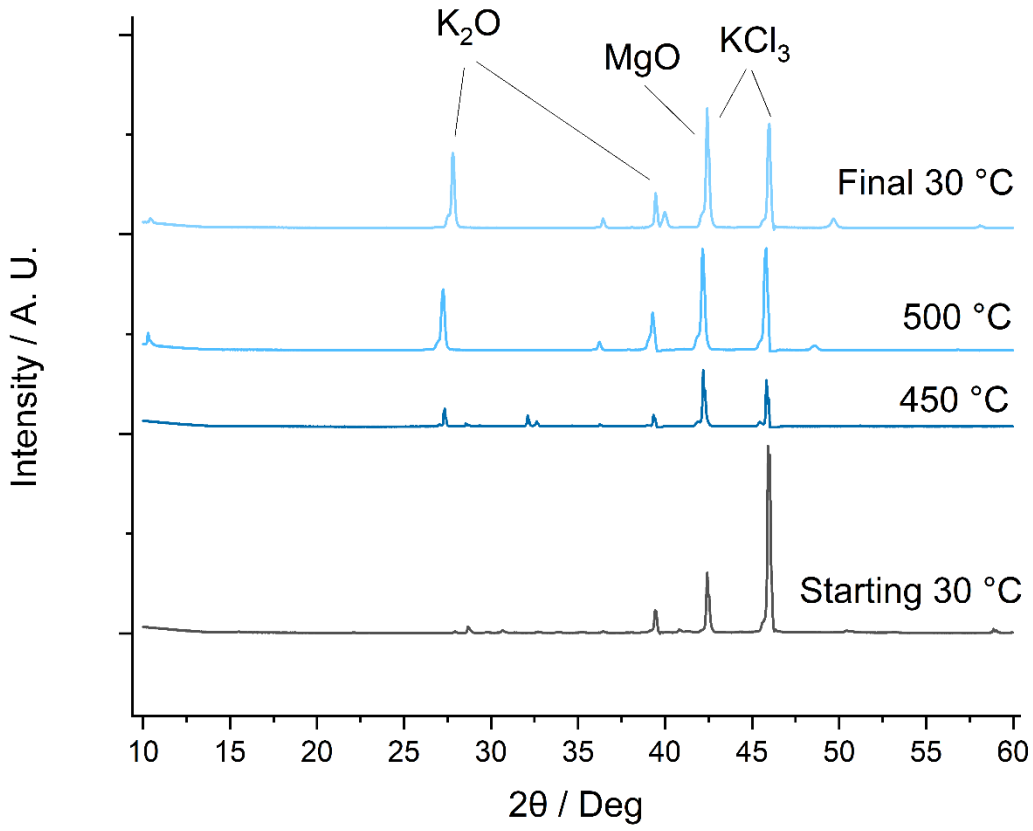

Figure 32: XRD spectra of KMgCl4357 with peak identification.

The sample source material from which the KMgCl4357 sample was drawn, was confirmed to be the correct ratio of $MgCl_2$ to KCl. The assumption can be made that the diffraction beam for the starting spectra did not have $MgCl_2$ in the preferred orientation to produce the peak. Subsequent peaks are presented in the later spectra. Potassium oxide and KCl_3 structures were present as temperature increased.

The statement can then be made, partnered with the results from the EGA experiments, that the chloride being released from the compound prior to the melting point is allowing the chemical reaction to take place and convert the ions of Mg^+ and K^+ to readily take up

any oxygen from atmospheric water or trace contaminants in the salts themselves. Carbon tape was used to pick up subsamples of the vapor trail and analyzed with LIBS and a scanning electron microscope energy-dispersive X-ray spectroscopy (SEM-EDS). Opening the sample chamber resulted in a rapid exposure to air after being held in helium and the vapor trails started to deliquesce, even when transferred to the carbon tape. Samples were taken quickly and then immediately stored in either a desiccator or glovebox and sealed in an inert environment before being transferred for analysis. LIBS and SEM analysis indicated $MgCl_2$ was emanating off as a vapor during the heating cycle. **Figure 33** shows a distinct vapor trail that was released from the pellet during the experiment.

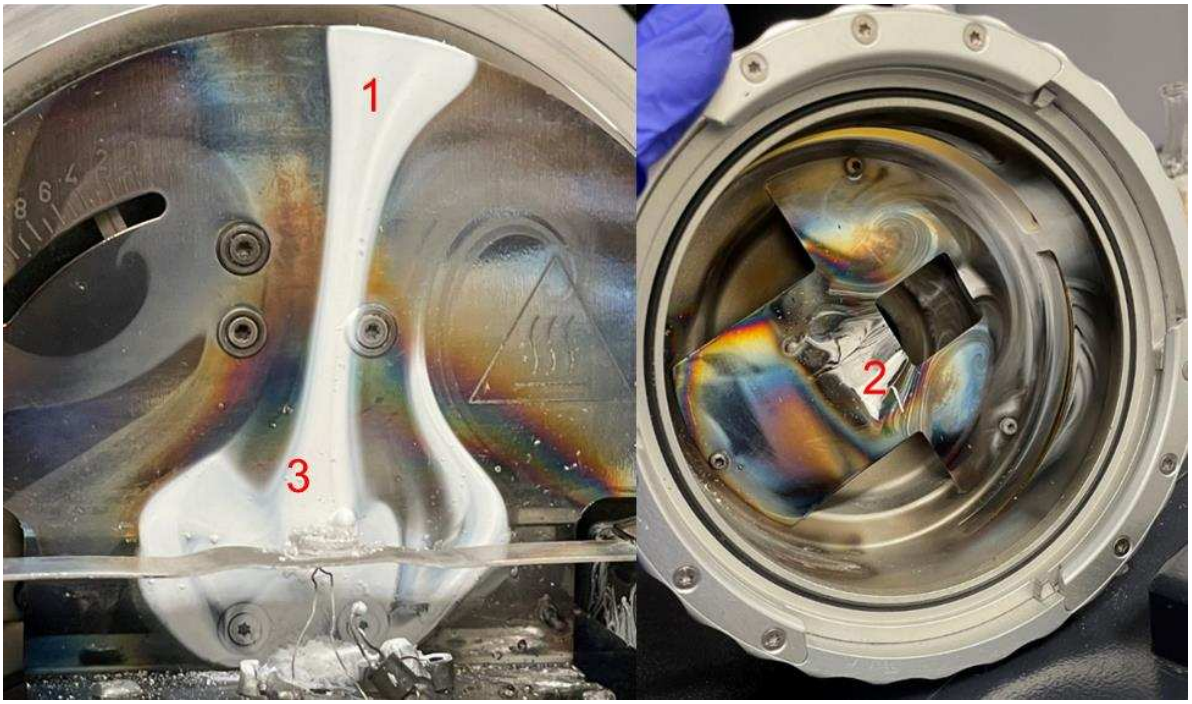

Figure 33: Vapor trail from $MgCl_2$ after completed scan on the front and back plate of the chamber.

This release was significant and resulted in little sample recovery, as the resulting trail once exposed to atmosphere immediately began deliquescing and the subsamples were taken to the glovebox for storage until needed for other analysis. The vapor was

subsampled in spots outlined in the figures using carbon tape to easily be transferred to other instruments (i.e., LIBS and SEM). The preliminary image produced from the SEM-EDS is an elemental map that shows the mixture or concentrations that were captured from the vapor trail (**Figure 34**).

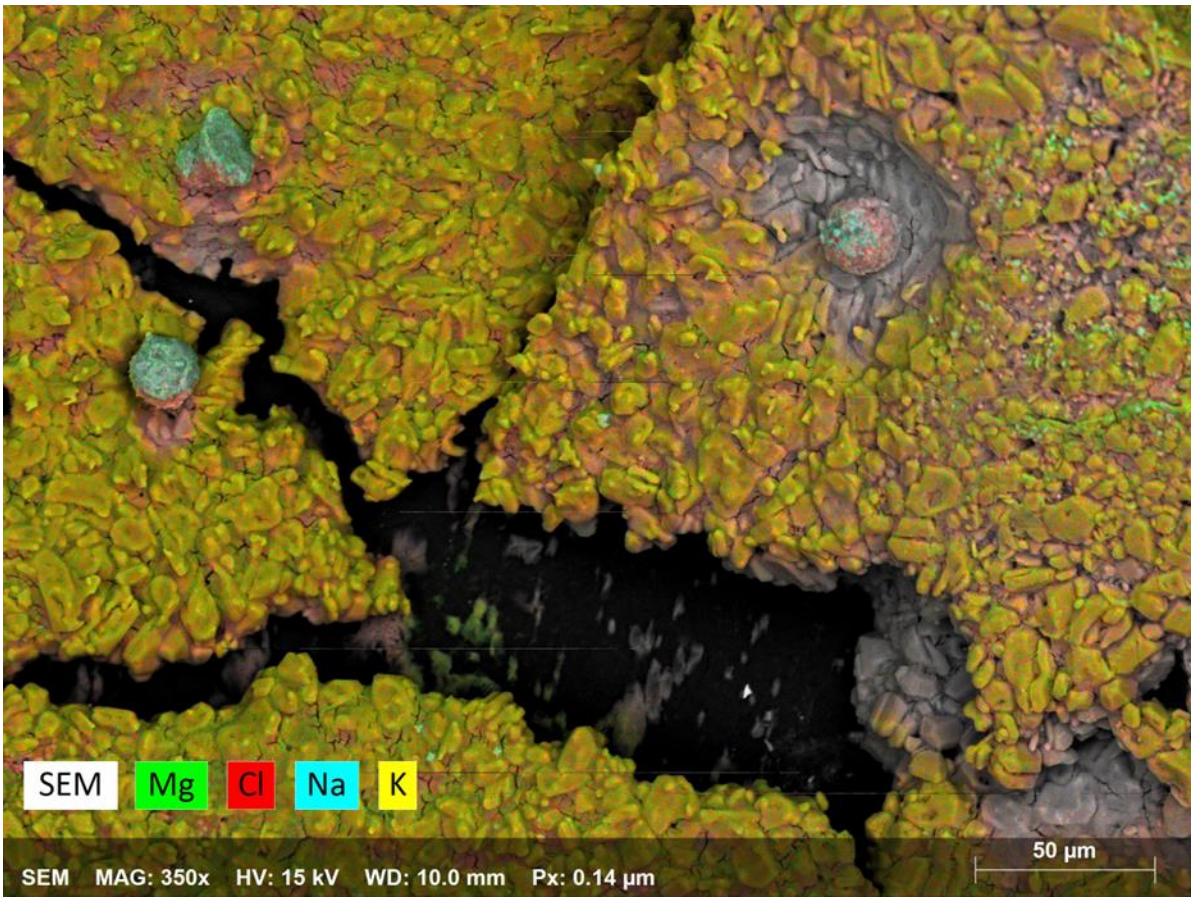

Figure 34: SEM-EDS results of the vapor trail collected from area 1 of Figure X at 350x magnification with a scale of 50 microns.

Magnesium, potassium, and chlorine were distributed throughout the condensed vapor indicating the salt is vaporizing as a salt and not in ionic or an elemental phase. The image appears to show the vapor trail had a higher concentration of $MgCl_2$ than KCl. Trace contamination of sodium is also present in circular crystals which could have been from exposure to atmosphere, contamination on the carbon tape or on the chamber backplate, and/or human intervention.

6.4 Heat Capacity and Enthalpy

6.4.1 Drop Calorimetry Materials and Methods

Preparation for the KMgCl samples was done in a similar way to that of the ClNaK series. Three empty nickel crucibles were welded using the operating parameters previously listed for the laser welder and used as the baseline drops. Along with the baseline crucibles, ultra-dry samples of each composition were batched in triplicate into nickel crucibles inside of a glovebox and press fitted before being transferred and laser welded. The same procedure was done for the off-the-shelf salts. Off-the-shelf salts were tested from 400 – 800°C and the ultra-dries were tested from 500 – 800°C. Potassium chloride data for the off-the-shelf salts was taken from the ClNaK experiments for the temperature range as the salt came from the same source material.

6.4.2 Results and Discussion

Following the fundamental trend, magnesium chloride increases in enthalpy as temperature increases which also results in the highest heat capacity value for the pure compound (**Figure 35**).

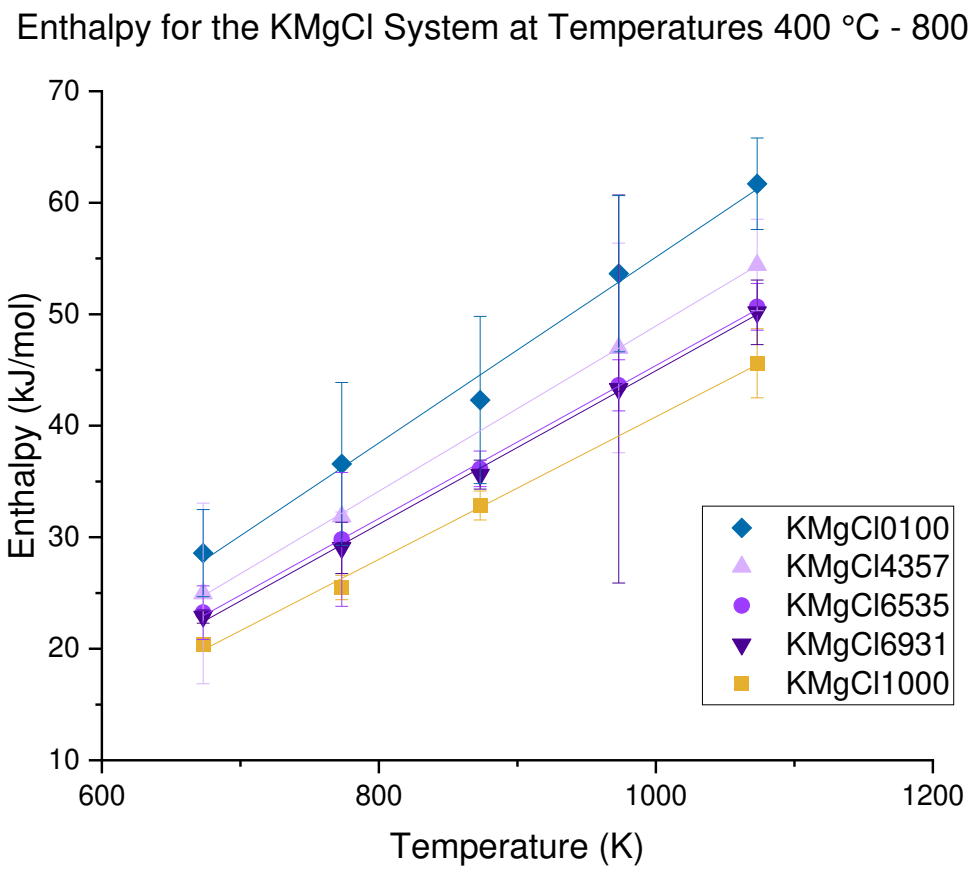

Figure 35: Enthalpy for the KMgCl system batched with off the shelf salts, uncertainty is two sigma.

Heat capacity values produced from the slope of enthalpy were compared to the simulated and experimental values presented in Lu[79]. to verify method and calculations for this specific system. Experimental values for the endpoints magnesium chloride and potassium chloride were determined to be 92.51 and 67.00 J/(mol·K), respectively.[79] The experimental values calculated for this study for the end members of magnesium chloride and potassium chloride were determined to be 84.0 and 64.2 J/(mol·K), respectively (**Table 16**).

Table 16: Linear trendline information with the determined heat capacity from the slope for the KMgCl system batched with off the shelf salts.

ClKMg	Slope (kJ/mol·K)	Intercept	Heat Capacity (J/mol·K)
1000	0.0642	-28.5946	64.2
6931	0.0707	-29.7964	70.7
6535	0.0712	-25.7283	71.2
4357	0.0817	-25.9917	81.7
0100	0.0840	-24.1162	84.0

The ultra-dry powders were packed, and hand pressed in inert atmosphere and had minimum exposure to the atmosphere before welding. The samples are assumed to be airtight. The results show the same trend as the off the shelf samples as shown in **Figure 36**.

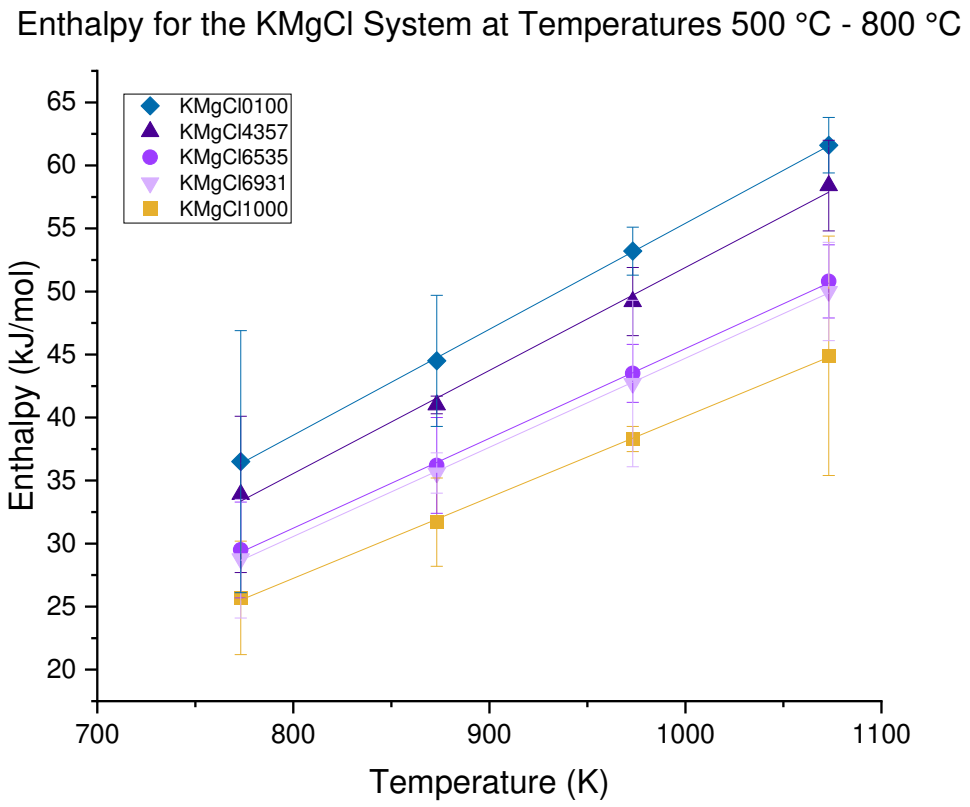

Figure 36: Enthalpy of KMgCl system from the ultra-dry batch of salts, uncertainty is two sigma.

The experimental values calculated for the ultra-dry magnesium chloride and potassium chloride were determined to be 83.8 and 62.5 J/(mol·K), respectively (**Table 17**).

Table 17: Linear trendline of ultra-dry KMgCl system from figure x and determined heat capacity.

ClKMg	Slope (kJ/mol·K)	Intercept	Heat Capacity (J/mol·K)
1000	0.0625	-22.686	62.5
6931	0.0688	-5.0904	68.8
6535	0.0687	-4.4968	68.7
4357	0.0740	-4.8622	74.0
0100	0.0838	-28.419	83.8

The recorded values for the wet salts are higher than those from the ultra-dry salts. Though the difference cannot be considered significant between the two salts, trace impurities, such as water content, can affect the measurement.

6.5 Conclusions

Studying the effects of water content on thermophysical properties examines the influence of how material is manufactured, packed, stored, and handled which became a large focal point for this work. The ultra-dry salts were assumed to have 0 wt% water contamination which was later discovered to be incorrect in the case of $MgCl_2$ via EGA and XRD results. Any water content in the $MgCl_2$ proved detrimental in all experiments conducted as the reaction to MgO was highly favorable. Magnesium oxide is a robust refractory material with a melting temperature of 2850°C which will prevent the molten salt from reaching a liquid phase or for conversion of $2MgCl_2 \rightarrow 2MgO + 2Cl_2$ to occur

during the lifetime of operation. Formation of MgO could result in the fuel or coolant no longer being able to function as a heat transfer material and invalidate the thermohydraulic calculations. The conversion to chlorine gas could result in a build-up of chlorine gas in any extra headspace which may lead to increased partial pressures in the core or piping. Purification and water content of the $MgCl_2$ will need to be thoroughly investigated if chosen as a fuel or coolant component. The potassium-magnesium chloride system appears to be less ideal as a coolant salt considering the volatile behavior of the eutectic compositions at elevated temperatures. Although, based on enthalpy and heat capacity the compositions with higher magnesium content will function better for reactor operation as they would be more stable as a heat exchanger. Vapor pressure and volatility, objectively, are of critical importance as the results affect all other thermophysical properties.

6.6 Future Work

Improvements have been made to the storage and handling of the material for the KMgCl and will continue to improve with each salt system or additional dopant. For future experiments, the salts should be massed by molar ratio as previously done and then melted in an inert atmosphere, crushed, and milled to mix and then remelted to ensure complete uniformity and mixing. The source composition and subsequent subsampling drawn from it will be in the ideal ratio when prepared properly per above. An exploratory study on mixing and the effects of volatility will need to be conducted. Verification of no changes in the salt ratio will be needed, even when all operations are conducted in an inert atmosphere. Absorbed water had a significant impact on many of the initial trials

throughout this study and will need to be further investigated. Salts from manufactures should be analyzed for initial water content; preliminary results show the water content varies from salt to salt anywhere between 1-5% water content. Ultra-dry samples doped with a known volume of water by weight percent will create a better matrix to aide in machine learning and adding in extra variables to understanding different salt systems. Future work will also include the doping of heavy metals at 300 ppm and 600 ppm into the KMgCl compositions to understand the effects of likely corrosion metals that will introduced to the system during the life of reactor operation. Batching of heavy metals will be done by weight percent rather than be included by molar percent to produce a more comparable matrix of experiment to reactor operation. The heavy metals chosen for this work, iron, chromium, and nickel, are all common and prevalent within the proposed structural material of the piping and core containment vessel. Preliminary testing has started on trace metal contaminant batches using the HTDC. Trace metal salts have breached several of the nickel crucibles and have leaked considerably during the drops. Further investigation of containment vessels for experiments and corrosion studies will need to be conducted to fully understand the heavy metal effects not only on the thermophysical properties but also to find a robust containment material that will have the longevity necessary for current proposed reactor life.

A new cold finger approach to understanding volatility is currently being explored using a tube furnace attached to the EGA. The tube furnace has a water-cooled pipe inserted, like that of the cooled backplate of the sample chamber in the XRD, which will collect and condense vapors being released from the salt. The vapor can then be scraped off the cold finger and analyzed using XRD to determine the ratio of phases or changes in

chemical species. LIBS will also be used to determine the amount of $MgCl_2$ or KCl that remains after the experiment has occurred. Refinement to this method will occur overtime to optimize running parameters and improve calculations.

Density will be investigated for the ultra-dry, increased water content, and trace metal samples for this work. A new method such as geometric benchtop pycnometry is currently under development and most recent results show good agreement with literature values. A thermomechanical analyzer (TMA) measures the displacement of a plunger from height A to height B during a heating profile to determine density of the salt at a target temperature. Trials were initially conducted using a custom, house-made nickel crucible, but due to the constant seizing of the plunger to the crucible a different design and crucible material needs to be investigated.

CHAPTER 7: CONCLUSIONS AND FUTURE WORK

7.1 Summary

Thermophysical properties remain the critical component to the thermohydraulic calculations to establish a functional molten salt reactor. This dissertation work provides a foundation to better understand and analyze complex salt systems through viable new methods. With sodium, potassium, and magnesium chloride being frontrunners as fuel and coolant salt components, intensive studies will need to be conducted to fully understand the multifaceted behavior of molten salts.

7.2 Batching, Handling, and Validation

Great improvements have been made between the original benchmark system of ClNaK and the refined focus of the KMgCl system. Batching ClNaK was done solely with a mortar and pestle with no validation on mixing or the ratio, whereas KMgCl ratio verification was done in triplicate for each batch made and prior to any further experimentation. Given the results from the EGA and XRD trials suggesting the eutectic compositions are volatilizing incongruently, validation is crucial for before and after trials to record the molar ratio that was measured if it had changed since beginning a heating profile.

Alongside ratio validation, optimal batching methods can be identified, such as the shatterbox versus a ball mill. The shatterbox, though not in an inert environment, is the fastest method available, mixes the best, and allows for a high quantity of sample to be prepared. The ball mill took three hours to produce similar results to the shatterbox and could only produce five-gram batches at a time.

Handling of the material was drastically different between the two salt systems because of the chemical reactions that occurred as well as the effects from trace impurities. For ClNaK, all experiments presented little to no evidence of negative impacts in relation to possible impurities in the salt and determined values were comparable to literature values. Water impurities had immediate impacts on KMgCl even prior to experiments as seen with the crust layer forming on XRD samples. The most significant impact resulted from the water content of the salt or exposure to atmosphere and the conversion of magnesium chloride to magnesium oxide during a heating profile. In the ultra-dry samples, only exposed to inert environments upon transferring to the necessary instrument per experiment, MgO was still observed. More refined studies of water content effects will need to be conducted to fully understand the negative, or perhaps positive impacts. Purification may become increasingly important depending on the salt system to ensure no trace impurities are present. The continued improvement of material handling, storage, and batching will result in a better understanding of speciation, phase changes, and effects on thermophysical properties.

7.3 High-Temperature Drop Calorimetry

The investigative studies from ClNaK were intensive in measurements, sampling, and materials used. Various types of crucibles in different sizes, shapes, styles, and materials were utilized until settling on the design drawn in Chapter five. A popular style was a crimped, toothpaste style capsule used for many experiments, but resulted in breached seals and salt leaks during the investigation. The KMgCl system was found to be more corrosive than ClNaK, which led to the exploration of the previous welding technique after

having several breached crucibles. The welding technique was adjust to shoot a pulse at the edge of the previous spot, resulting in a better overlap and a more penetrative weld. Improved welding technique significantly reduced the breach of salt during the drop calorimetry experiments. The method was validated using literature values for the enthalpy and heat capacity as previously mentioned.

The HTDC and welded crucibles have the potential to provide excellent information on corrosion effects on proposed construction materials that will contain the reactor core. The HTDC can be set to proposed operating temperatures or create hot/cold spots that could be present in the core if the heat is not uniformly distributed by setting the 3 zones to varied temperatures. Different crucibles of proposed containment material can also be fabricated to hold fuel or coolant salts. A concurrent experiment on welding the crucible can be conducted as well. Welding experiments will also provide information on the structural strength of proposed containment materials that could tie into longevity studies.

7.4 Vapor Pressure and Volatility

More exploratory studies were conducted using KMgCl to understand the complexities of phase changes and chemical evolutions when in volatile states. The original method discussed in Chapter five used results from TGA and EGA, which worked well for the ClNaK system, KMgCl had a clear affinity to convert $2MgCl_2 \rightarrow 2MgO + 2Cl_2$. Potassium-magnesium chloride highlighted the importance in understanding the salt species that can form during the transition to liquid phase. The TGA provided valuable information and is often used in vapor pressure studies for other materials.[63, 84] Having a validated method that accurately determines the rate of volatilization will be crucial when determining a

correction factor that can be applied to other experiments. The hypothesis behind the use of a correction factor will be to accurately determine what molar percent the salt composition would be depending on the conditions it has undergone. Coupled with the TGA, the EGA experiments allow for the identification of salt speciation as vapors are released, a vital component to fuel qualification and reactor design as the potential changes in starting material could shutdown the reactor. X-ray diffraction furthers characterization methods for fuel and coolant compositions, with the hotstage providing essential information during the melting process. Experiments coupling the three instruments will allow for the determination of effects of trace impurities, identify phase changes and formation of different compounds, salt behavior through proposed reactor operations, and provide a correction for all other thermophysical experiments.

7.5 Density

Benchtop gravimetric pycnometry is an inexpensive, rugged method to determine density of salt forms; however, was only tested using the complete matrix of ClNaK. A single preliminary experiment was conducted using the KMgCl system and the results were catastrophic (**Figure 37**).

Figure 37: Resulting KMgCl6931 after benchtop geometric pycnometry experiment.

The KMgCl6931 formed a hard crusted surface similar to the samples that were prepped for the XRD, with no appearance of a complete melt. The sample lost significant mass and the furnace components were coated with layers of salt. Due to the concerning results, further investigation needs to be done to confirm the method validity with more complex systems.

The preliminary results from the thermomechanical analyzer or displacement method have shown promise when compared to models and literature values. The thermomechanical analyzer is more calibrated than the geometric benchtop pycnometry method and uses less sample – which will be safer when high activity actinides are studied. Benchtop instruments have a higher risk of salt damaging the internal components of the instrument when not contained properly. Further studies will need to be conducted on the reproducibly to see if, over time, there is a change in measurement or instrumental output that could correlate to salt impact.

REFERENCES

(1) Nuclear Regulatory Commission. *Power Reactors*. 2022. https://www.nrc.gov/reactors/power.html (accessed.

(2) Termini, N.; Birri, A.; Henderson, S.; Ezell, N. D. B. *An Overview of the Molten Salt Thermal Properties Database–Thermophysical, Version 2.1.1 (MSTDB-TP v.2.1.1)*; Oak Ridge National Laboratory, 2023. DOI: https://doi.org/10.2172/1988348.

(3) Chartrand, P.; Pelton, A. D. Thermodynamic evaluation and optimization of the Li, Na, K, Mg, Ca//F, Cl reciprocal system using the modified quasi-chemical model. *Metallurgical and Materials Transactions A* **2001**, *32*, 1417-1430.

(4) McMurray, J.; Johnson, K.; Agca, C.; Betzler, B.; Kropaczek, D.; Besmann, T.; Andersson, D.; Ezell, N. *Roadmap for thermal property measurements of Molten Salt Reactor systems*; Oak Ridge National Laboratory, 2021.

(5) Karfidov, E.; Nikitina, E.; Erzhenkov, M.; Seliverstov, K.; Chernenky, P.; Mullabaev, A.; Tsvetov, V.; Mushnikov, P.; Karimov, K.; Molchanova, N.; et al. Corrosion Behavior of Candidate Functional Materials for Molten Salts Reactors in LiF–NaF–KF Containing Actinide Fluoride Imitators. *Materials* **2022**, *15*.

(6) Huang, Q.; Lu, G.; Wang, J.; Yu, J. Thermal decomposition mechanisms of $MgCl_2 \cdot 6H_2O$ and $MgCl_2 \cdot H_2O$. *Journal of Analytical and Applied Pyrolysis* **2011**, *91*, 159-164.

(7) Hartmann, T.; Paviet, P. Corrosion of Containment Alloys in Molten Salt Reactors and the Prospect of Online Monitoring. *Journal of Nuclear Fuel Cycle and Waste Technology* **2021**.

(8) Betzler, B. R.; Heidet, F.; Feng, B.; Rabiti, C.; Sofu, T.; Brown, N. R. Modeling and simulation functional needs for molten salt reactor licensing. *Nuclear Engineering and Design* **2019**, *355*. DOI: ARTN 110308 10.1016/j.nucengdes.2019.110308.

(9) Glazoff, M.; Charit, I.; Sabharwall, P. *Computational Thermodynamic Modeling of Hot Corrosion of Alloys Haynes 242 and Hastelloy^{TM}N for Molten Salt Service*; Idaho National Laboratory, 2014.

(10) McFarlane, J.; Taylor, P.; Holcomb, D. E.; Poore, I., W.P. *Review of Hazards Associated with Molten Salt Reactor Fuel Processing Operations*; Oak Ridge National Lab, 2019.

(11) Serp, J.; Allibert, M.; Benes, O.; Delpech, S.; Feynberg, O.; Ghetta, V.; Heuer, D.; Holcomb, D.; Ignatiev, V.; Kloosterman, J. L.; et al. The molten salt reactor (MSR) generation IV: Overview and perspectives *Progress in Nuclear Energy* **2014**, *77*, 308-319.

(12) Uhlir, J. Chemistry and technology of Molten Salt Reactors - history and perspectives. *Journal of Nuclear Materials* **2007**, *360* (1), 6-11. DOI: 10.1016/j.jnucmat.2006.08.008.

(13) Ewing, C. T.; Stern, K. H. Equilibrium Vaporization Rates and Vapor Pressures of Solid and Liquid Sodium Chloride, Potassium Chloride, Potassium Bromide, Cesium Iodide, and Lithium Fluoride. *Naval Research Laboratory* **1974**.

(14) Moon, J.; Andrews, H.; Agca, C.; Bilheux, J.-C.; Braatz, A.; McAlister, A.; McFarlane, J.; McMurray, J.; Robb, K.; Zhang, Y. Density Measurements of Various Molten Sodium, Magnesium, Potassium, and Uranium Chloride Salt Compositions Using Neutron Imaging. *Industrial Engineering & Chemistry* **2022**, *61* (48), 17665-17673.

(15) Kirshenbaum, A. D.; Cahill, J. A.; McGonigal, P. J.; Grosse, A. V. The density of liquid NaCl and KCl and an estimate of their critical constants together with those of the other alkali halides. *Journal of Inorganic and Nuclear Chemistry* **1962**, *24* (10), 1287-1296. DOI: https://doi.org/10.1016/0022-1902%2862%2980205-X.

(16) Can, Y.; Acar, B. B. Nuclear proliferation resistance assessment of fuel cycles closed with complete co-processing of spent fuel. *Progress in Nuclear Energy* **2022**.

(17) IEA. *Global Energy Review: CO2 Emissions in 2021*; Paris, 2022. https://www.iea.org/reports/global-energy-review-co2-emissions-in-2021-2.

(18) U.S. Energy Information Administration. *Electrcity explained*. 2022. https://www.eia.gov/energyexplained/electricity/electricity-in-the-us.php (accessed.

(19) Hazboun, S. O.; Boudet, H. S. Public Preferences in a Shifting Energy Future: Comparing Public Views of Eight Energy Sources in North America's Pacific Northwest. **2020**, *13*.

(20) Grid Deployement Office. *What does it take to modernize the U.S. electric grid?* . 2023. (accessed 2024.

(21) Office of Electricity. *Grid Modernization and the Smart Grid*. 2024. (accessed 2024.

(22) Grid Deployement Office. *Grid Resilience and Innovation Partnerships (GRIP) Program*. 2024. (accessed.

(23) United Nations. *What is renewable energy?* . 2024. (accessed 2024.

(24) Johlas, H.; Witherby, S.; Doyle, J. R. Storage requirements for high grid penetration of wind and solar

power for the MISO region of North America: A case study. *Renewable Energy* **2019**, *146*, 1315-1324.

(25) Lee, C.-C.; Maron, M.; Mostafavi, A. Community-scale big data reveals disparate impacts of the Texas winter storm of 2021 and its managed power outage. *Humanities and Social Sciences Communications* **2022**, *9* (1). DOI: 10.1057/s41599-022-01353-8.

(26) National Centers for Environmental Information. *The Great Texas Freeze: February 11-20, 2021*. NOAA, 2023. https://www.ncei.noaa.gov/news/great-texas-freeze-february-2021#:~:text=On%20February%2011%2D20%2C%202021,the%20entire%20state%20of%20Texas. (accessed 2024.

(27) Rives, K. Hydro plants in US West boost production 13% in 2021-2022. *SNL Energy Power Daily* **2023**. ABI/INFORM Trade & Industry.

(28) Dreves, H. *How Extreme Weather and System Aging Affect the US Photovoltaic Fleet*. 2024. (accessed.

(29) United Nations. The Paris Agreement. UN, Ed.; 2015.

(30) The White House. Fact Sheet: The American Jobs Plan 2021.

(31) Allardice, C.; Trapnell, E. R. The First Pile. United States Atomic Energy commission,: 1946.

(32) Office of Nuclear Energy. *Nuclear is the Most Reliable Energy Source and It's Not Even Close*. 2022. https://www.energy.gov/ne/articles/nuclear-power-most-reliable-energy-source-and-its-not-even-close (accessed.

(33) Baron, J.; Herzog, S. Public opinion on nuclear energy and nuclear weapons: The attitudinal nexus in the United States. *Energy Research & Social Science* **2020**, *68*.

(34) Cornfield, J. *WA governor urged to veto $25M for nuclear power project*. WA State Standard, 2024. (accessed.

(35) Nuclear Regulatory Commission. *Pressurized Water Reactors*. 2023. https://www.nrc.gov/reactors/power/pwrs.html (accessed.

(36) Nuclear Regulatory Commission. *Boiling Water Reactors*. 2023. https://www.nrc.gov/reactors/power/bwrs.html (accessed.

(37) Office of Nuclear Energy. *5 Fast Facts about Spent Nuclear Fuel*. 2022. (accessed.

(38) DOE Loan Programs Office. *Vogtle*. 2019. (accessed 2024.

(39) Georgia Power. *Vogtle Unit 4 connects to electric grid for the first time*. 2024. (accessed 2024.

(40) IAEA. *Spent Fuel Reprocessing Options*; IAEA-TECDOC-1587; IAEA, Vienna, Austria, 2008.

(41) IAEA. *Status and Advances in MOX Fuel Technology*; STI/DOC/010/415; Vienna, 2003.

(42) Bevard, B. B.; Ellis, R. J.; Howard, R. L.; Fisher, S. E.; Joseph III, R. A. *The Use of MOX Fuel in the United States: Bibliography of Important Documents and Discussion of Key Issues*; ORNL/LTR-2012/315; Oak Ridge National Laboratory, Oak Ridge, 2012.

(43) Hartmann-Paviet, P.; Cerefice, G.; Stacey, M. R.; Bakhtiar, S. *Analysis of Nuclar Proliferation Resistance Reprocessing and Recycling Technologies*; Idaho National Lab, 2011.

(44) Chandler, J.; Hertel, N. Choosing a reprocessing technology requires focusing on what we value. *Progress in Nuclear Energy* **2009**, 701-708.

(45) Erickson, R.; Abney, K.; Dale, D. *Aqueous polishing of plutonium oxide for mixed-oxide fuel*; Los Alamos National Laboratory 2000.

(46) Elsheikh, B. M. Safety Assessment of molten salt reactors in comparison with light water reactors. *Journal of Radiation Research and Applied Sciences* **2013**, *6* (2), 63-70.

(47) Ho, A.; Memmott, M.; Hedengren, J.; Powell, K. M. Exploring the benefits of molten salt reactors: analysis of flexibility and safety features using dynamic simulation. *Digital Chemical Engineering* **2023**, *7*.

(48) Roper, R.; Harkema, M.; Sabharwall, P.; Riddle, C.; Chisholm, B.; Day, B.; Marotta, P. Molten salt for advanced energy applications: A review. *Annals of Nuclear Energy* **2022**, *169*.

(49) Noorie-kalkhoran, O.; Litskevich, D.; Detkina, A.; Jain, L.; Carland-Glover, G.; Merk, B. On the Employment of a Chloride or Fluoride Salt Fuel System
in Advanced Molten Salt Reactors, Part 1: Thermophysical
Properties and Core Criticality. *Energies* **2022**, *15*.

(50) IAEA. *Molten Salt Reactors*. iaea.org/topics/molten-salt-reactors (accessed.

(51) Barton, J. L.; Bloom, H. A Boiling Point Method for Determination of Vapor Pressures of Molten Salts. *Journal of Physical Chemsitry* **1956**.

(52) Rodebush, W. H.; Dixon, A. L. The Vapor Pressures of Metals; A New Experimental Method. *Vapor Pressure of Metals* **1925**.

(53) Flanagan, G. F.; Holcomb, D. E.; Poore, I., W.P. *Molten Salt Reactor Fuel Qualification Considerations and Challenges*; Oak Ridge National Lab, 2018.

(54) Zakiryanov, D. The impact of oxide impurity on the structure of FLiNaK and FLiNaK–CeF3 melts: A simulation study. *Journal of Molecular Liquids* **2023**, *384*.

(55) Yan, Y.; Li, Y.; Fu, H.; Qian, Y.; Li, Q.; Dou, Q.; Geng, J. Effect of oxide impurities on the dissolution

behavior of Th^{4+}, Be^{2+} and U^{4+} in fluoride salts. *Royal Society of Chemistry* **2023**, *14*.

(56) Mausolff, Z.; DeHart, M.; Goluoglu, S. Design and assessment of a molten chloride fast reactor. *Nuclear Engineering and Design* **2021**, *379*.

(57) Severino, J.; Jacob, R.; Belusko, M.; Liu, M.; Bruno, F. A novel, low-cost and robust method for determining molten salt density at high temperatures. *Journal of Energy Storage* **2021**, *41*. DOI: ARTN 102935

10.1016/j.est.2021.102935.

(58) Agca, C.; McMurray, J. Emperical estimation of densities in NaCl-KCl-UCl_3 and NaCl-KCl-YCl_3 molten salts using Redlich-Kister expansion. *Chemical Engineering Science* **2022**, *247*.

(59) Parker, S. S.; Long, A. M.; Carver, D. T.; Jackson, J. M.; Monreal, M. J. *Density Measurement of NaCl-MgCl2-PuCl3 and NaCl-UCl3-PuCl3 Molten Salt Systems by Neutron Radiographic Dilatometry*; Los Alamos National Lab, 2023.

(60) Miller, R. C.; Kursch, P. Molecular Composition of Alkali Halide vapors. *The Journal of Chemical Physics* **1955**.

(61) Barchuck, V. T.; Dubovoi, P. G. Measurement of a Saturated Vapor Pressure Over Highly Volitile Salt Melts. *Ukr. Khim. Zh. (Russ. Ed.)* **1973**, *39* (8), 838-840.

(62) Atkins, P.; Paula, J. d. *Physical Chemistry*; 2006.

(63) Wright, S. F.; Dollimore, D.; Dunn, J. G.; Alexander, K. Determination of the vapor pressure curves of adipic acid and triethanolamine using thermogravimetric analysis. *Thermochimica Acta* **2004**, *421* (1-2), 25-30. DOI: 10.1016/j.tca.2004.02.021.

(64) Hatton, P.; Lundie, D. Mass Spectrometry in Real Time. In *Labmate*, Analytical, H., Ed.; UK & Ireland, 2020.

(65) Skoog, D. A.; Holler, J. E.; Crouch, S. R. *Principles of Instrumental Analysis*; David Harris, 2007.

(66) Hiden Analytical. *HPR-20 R&D*. 2021. (accessed.

(67) NIST Chemistry WebBook, SRD 69 - Sodium Chloride. (accessed.

(68) NIST. NIST Chemistry WebBook, SRD 69 - Potassium Chloride. **1974**.

(69) NIST Chemistry WebBook SRD 69 - Magnesium Chloride. (accessed.

(70) NIST-JANAF Themochemical Tables (Nickel). NIST. (accessed.

(71) *Product Sheet XRD 45: D8 Discover Plus*; Bruker.

(72) Bruker AXS GmbH. *D8 Series User Manual*; DOC-M88-EXX153 V6; Federal Republic of Germany, 2018.

(73) West, A. R. *Basic Solid State Chemistry*; John Wiley & Sons, 1999.

(74) David, W. I. F.; Shankland, K.; McCusker, L. B.; Baerlocher, C. *Structure Determination from Powder Diffraction Data*; Oxford University Press, 2002.

(75) Villada, C.; Ding, W.; Bonk, A.; Bauer, T. Engineering molten MgCl2–KCl–NaCl salt for high-temperature thermal energy storage: Review on salt properties and corrosion control strategies. *Solar Energy Materials and Solar Cells* **2021**, *232*.

(76) Turchi, C. S.; Vidal, J.; Bauer, M. Molten salt power towers operating at 600–650 °C: Salt selection and cost benefits. *Solar Energy* **2018**, *164*, 38-46.

(77) Pan, G.; Ding, J.; Wang, W.; Lu, J.; Li, J.; Wei, X. Molecular simulations of the thermal and transport properties of alkali chloride salts for high-temperature thermal energy storage. *International Journal of Heat and Mass Transfer* **2016**, *103*, 417-426.

(78) Hanson, K.; Sankar, K. M.; Weck, P. F.; Startt, J. K.; Dingreville, R.; Deo, C. S.; Sugar, J. D.; Singh, P. M. Effect of excess Mg to control in molten $MgCl_2$ and KCl eutectic salt mixture. *Corrosion Science* **2022**, *194*.

(79) Lu, J.; Yang, S.; Rong, Z.; Pan, G.; Ding, J.; Liu, S.; Wei, X.; Wang, W. Thermal properties of KCl-$MgCl_2$ eutectic salt for high-temperature heat transfer and thermal storage system. *Solar Energy Materials and Solar Cells* **2021**, *228*.

(80) Sun, H.; Wang, J.-Q.; Tang, Z.; Liu, Y.; Wang, C. Assessment of effects of Mg treatment on corrosivity of molten NaCl-KCl-$MgCl_2$ salt with Raman and Infrared spectra. *Corrosion Science* **2020**, *164*.

(81) Xu, X.; Wang, X.; Li, P.; Li, Y.; Hao, Q.; Xiao, B.; Elsentriecy, H.; Gervasio, D. Experimental Test of Properties of KCl–$MgCl_2$ Eutectic Molten Salt for Heat Transfer and Thermal Storage Fluid in Concentrated Solar Power Systems. *Journal of Solar Energy Engineering* **2018**, *140*.

(82) Applied Spectra. *What is LIBS?* . 2023. (accessed.

(83) Dass, C. *Fundamentals of Contemporary Mass Spectrometry*; John Wiley & Sons, 2007.

(84) Price, D. M. Vapor pressure determination by thermogravimetry. *Thermochimica Acta* **2001**, *367*.

APPENDIX

Table 18: Raw data for Figure 16

Temperature (°C)	Average (g/cm^3)	Uncertainty (g/cm^3)	Percent Error (%)
800	1.87	0.07	22.5
850	1.34	0.0003	10.8
900	1.49	0.08	0.9
950	1.43	0.01	1.5
1000	1.38	0.09	3.3

Table 19: Raw data for Figure 17

Temperature (°C)	Average (g/cm^3)	Uncertainty (g/cm^3)	Percent Error (%)
800	1.66	0.02	9.5
850	1.28	0.04	14.1
900	1.55	0.03	5.8
950	1.35	0.03	6.3
1000	1.34	0.07	5.3

Table 20: Raw data for Figure 19 - enthalpy end points

Temperature (K)	ClNaK10000 (kJ/mol)	Uncertainty (kJ/mol)	ClNaK00100 (kJ/mol)	Uncertainty (kJ/mol)
573.15	14.7	2.6	14.8	1.6
673.15	20.0	1.4	20.4	1.0
763.15	25.1	1.5	25.5	2.1
783.15	26.3	1.2	26.7	1.3
823.15	28.6	2.1	29.3	2.6
863.15	31.0	1.8	31.6	2.3
883.15	32.2	3.5	32.8	2.2
1063.15	42.9	5.2	53.5	3.7
1083.15	44.8	2.8	44.8	3.3
1163.15	49.9	4.0	52.9	9.7
1173.15	50.7	8.1	53.4	10.9
1183.15	51.8	2.7	54.3	8.3
1223.15	54.4	6.5	56.8	7.5

Table 21: Raw Data for Figure 19 – enthalpy mixed compositions

Temperature (K)	ClNaK7525 (kJ/mol)	Uncertainty (kJ/mol)	ClNaK5149 (kJ/mol)	Uncertainty (kJ/mol)	ClNaK2575 (kJ/mol)	Uncertainty (kJ/mol)
573.15	14.8	1.2	14.8	0.8	14.8	1.3
673.15	20.1	1.4	20.1	1.7	20.3	2.1
763.15	25.3	2.7	25.3	3.1	25.6	2.5
783.15	26.3	3.2	26.4	2.2	26.7	2.4
823.15	28.6	2.2	28.7	2.4	29.0	2.3
863.15	31.0	3.7	31.1	3.2	31.5	3.3
883.15	32.2	3.1	32.4	2.6	32.7	3.6
1063.15	41.2	9.0	41.1	4.5	41.3	6.8
1083.15	43.7	3.6	44.3	7.1	59.9	5.3
1163.15	44.9	3.7	44.9	3.7	45.2	5.0
1173.15	50.4	5.2	50.5	3.4	50.9	6.4
1183.15	51.4	6.0			51.4	8.9
1223.15	51.6	7.0	52.4	4.4	52.7	6.9

Table 22: Raw data for Figure 22.

Time (hrs)	Temperature (°C)	NaCl (ppm)	KCl (ppm)	ClNaK5149 (ppm)
0.62	264	0.150	-0.018	-0.016
0.77	355	0.208	0.110	-0.047
0.96	466	0.277	-0.169	-0.119
1.16	586	0.322	-0.086	-0.088
1.29	664	0.425	0.021	0.071
1.50	790	0.470	0.103	-0.225
1.67	893	0.515	0.128	0.083
1.96	950	0.565	0.032	0.066
2.09	950	0.669	0.025	-0.056

Table 23: Raw data for Figure 24.

KCl (mol%)	Average (K/Cl)	Uncertainty (K/Cl)	RSD
0	0.35	0.04	11.6
43	7.58	2.01	26.5
65	12.53	1.65	13.2
69	14.31	1.74	12.2
100	14.68	1.33	9.0

Table 24: Raw data for Figure 35.

Temperature (K)	KMgCl1000 (kJ/mol)	Uncertainty (kJ/mol)	KMgCl4357 (kJ/mol)	Uncertainty (kJ/mol)	KMgCl6535 (kJ/mol)	Uncertainty (kJ/mol)	KMgCl6931 (kJ/mol)	Uncertainty (kJ/mol)	KMgCl0100	Uncertainty (kJ/mol)
673.15	20.4	0.5	25.0	8.1	23.2	2.4	22.9	0.6	28.6	3.9
773.15	25.5	1.1	31.9	0.4	29.8	6.0	29.0	2.3	36.6	7.3
873.15	32.8	1.3			36.1	1.6	35.6	1.3	42.3	7.5
973.15			47.0	9.4	43.6	2.3	43.3	17.4	53.6	7.0
1073.15	45.6	3.1	54.4	4.1	50.7	2.1	50.2	2.9	61.7	4.1

Table 25: Raw data for Figure 36.

Temperature (K)	KMgCl1000 (kJ/mol)	Uncertainty (kJ/mol)	KMgCl4357 (kJ/mol)	Uncertainty (kJ/mol)	KMgCl6535 (kJ/mol)	Uncertainty (kJ/mol)	KMgCl6931 (kJ/mol)	Uncertainty (kJ/mol)	KMgCl0100	Uncertainty (kJ/mol)
773.15	25.7	4.5	33.9	6.2	29.5	3.8	28.8	4.7	36.5	10.4
873.15	31.7	3.5	41.0	0.7	36.2	3.8	35.6	1.6	44.5	5.2
973.15	38.3	1.0	49.2	2.7	43.5	2.3	42.7	6.6	53.2	1.9
1073.15	44.9	9.5	58.4	3.6	50.8	2.9	50.0	3.9	61.6	2.2

LIST OF ACRONYMS, ABBREVIATIONS, AND SYMBOLS

ANP	Aircraft Nuclear Propulsion Program
BWR	Boiling Water Reactor
DOE	Department of Energy
DOE-NE	Department of Energy Office of Nuclear Energy
DSC	Differential Scanning Calorimetry
EGA-MS	Evolved Gas Analysis - Mass Spectrometry
GIF	Generation IV International Forum
GRIP	Grid Resilience and Innovation Partnerships
TXS-HE	High Efficiency Turbo X-ray Source
HFIR	High Flux Isotope Reactor
HTDC	High-temperature Drop Calorimeter
ICP-OES	Induced-coupled Plasma Optical Emission Spectroscopy
JANAF	Joint-Army-Navy-Air Force
LIBS	Laser Induced Breakdown Spectroscopy
LWR	Light Water Reactor
LANSCE	Los Alamos Neutron Science Center
MOX	Mixed-oxide Fuel
MSR	Molten Salt Reactor
MSRE	Molten Salt Reactor Experiment
MSTDB-TP	Molten Salt Thermal Properties Database – Thermal Physical

NIST	National Institute of Standards and Technology
NMR	Nuclear Magnetic Resonance
ORNL	Oak Ridge National Laboratory
KMgCl	Potassium-magnesium Chloride
PWR	Pressurized Water Reactor
QIC	Quartz Inert Capillary
RK	Redlich-Kister
RGA-MS	Residual Gas Analysis - Mass Spectrometry
SEM	Scanning Electron Microscopy
SEM-EDS	Scanning Electron Microscopy Energy-dispersive X-ray Spectroscopy
SFR	Sodium-cooled Fast Reactor
ClNaK	Sodium-potassium Chloride
TGA	Thermogravimetric Analyzer
TMA	Thermomechanical Analyzer
TRU	Transuranic
XRD	X-ray Diffraction